COO-3077-102
MF-84

Courant Institute of

Mathematical Sciences

Magneto-Fluid Dynamics Division

On Supplementary Heating of Fusion Plasmas by Means of Alfvén Waves

J. A. Tataronis and W. Grossmann

U.S. Energy Research and Development Report

Plasma Physics
September 1977

New York University

UNCLASSIFIED

New York University

Courant Institute of Mathematical Sciences

Magneto-Fluid Dynamics Division

MF-84 COO-3077-102

ON SUPPLEMENTARY HEATING OF FUSION PLASMAS BY MEANS OF ALFVÉN WAVES

J. A. Tataronis and W. Grossmann

September 1977

U.S. Energy Research And Development Administration

Contract No. EY-76-C-02-3077*000

UNCLASSIFIED

Abstract

A comprehensive treatment of the theory of rf energy absorption in inhomogeneous plasmas by means of Alfvén waves is presented. A straight cylindrical plasma column whose motion is governed by linearized ideal magnetohydrodynamics (MHD) is assumed to be surrounded by a vacuum region in which an ideal coil consisting of surface currents is placed. The coil is oscillated at frequencies which lie in the MHD continuous spectrum of local Alfvén frequencies of the inhomogeneous plasma leading to the occurrence of local Alfvén resonances. A rigorous self-consistent analysis of the resulting resonant energy absorption is presented along with calculations relevant to present and future fusion devices. Specifically, the experimentally useful coil impedance is calculated for a plasma-vacuum-coil-wall system with realistic nonuniform plasma profiles corresponding to present day Tokamak and Scyllac devices. Impressively large coupling and absorption is indicated for such devices independent of the value of total plasma β. Significant differences occur however for variations in the spatial plasma profiles. Consequently accurate scaling estimates of Alfvén wave absorption are not possible without solving the complete nonuniform problem.

1. Introduction

One of the most important problems facing the development of Tokamak fusion plasma experiments is the effective plasma heating over and above that obtainable from Joule heating. This paper addresses itself to this problem. In particular, calculations are presented for a new heating mechanism which may be more attractive than current conventional techniques.

Of the many candidates for Tokamak heating which are currently in vogue are neutral beam injection and rf plasma heating at ion cyclotron (ICRH) and lower hybrid frequencies (LHRH). Neutral beam injection has proven effective in small machines such as the ATC and ORMAK where the beam only produces small perturbations on the background plasma equilibrium. Fusion plasma experiments, on the other hand, due to the very large beam energy and currents, may be significantly disturbed by the beam such that the equilibrium would be altered. Ion cyclotron resonant heating has also been shown to work in the ST plasma. The rf power densities in the ST experiment were of the order of 100 kw, and significant ion heating was observed. Extrapolating again to fusion plasma parameters, it is questionable whether such large rf energies can be generated at the necessary high frequencies. From the standpoint of minimum disturbance of the plasma it would be very attractive to be able to couple rf energy into a fusion plasma at technically reasonable frequencies. The main contribution of the present work to the subject of plasma heating is to

document computations which support the assertion that rapid rf energy absorption and eventual plasma heating in thermonuclear devices may be produced at frequencies several orders of magnitude less than the ion cyclotron frequency through the excitation of Alfvén waves. A secondary contribution is to provide a comprehensive review of the theoretical foundations of this absorption and heating mechanism.

The heating of plasmas by Alfvén waves was actually proposed earlier by Furth (1959). This early proposal had the disadvantage of requiring that the wave generator be imbedded in the plasma, a condition which is clearly unreasonable for thermonuclear plasmas. Recently though, several authors (Grossmann and Tataronis, 1973; Tataronis and Grossmann, 1974; Tataronis, 1975; Kappraff, Tataronis and Grossmann, 1975; Tataronis and Grossmann, 1976; Tataronis and Kappraff, 1977; Chen and Hasegawa, 1974) have considered an alternative approach to heat plasmas by means of Alfvén wave excitation. The physics of this new approach can best be understood by considering the plasma to be a perfectly conducting magnetohydrodynamic (MHD) fluid with profiles inhomogeneous in the direction perpendicular to the magnetic flux surfaces. As shown elsewhere (Tataronis and Grossmann, 1971, 1972; Uberoi, 1972), Alfvén waves in the MHD model propagate locally on magnetic flux surfaces, and have a phase velocity which varies in space according to the spatial variations of the plasma profiles. This local variation in the Alfvén phase velocity and the fact that Alfvén wave propagation is one dimensional along the magnetic flux surfaces together imply the

existence of a continuous spectrum of Alfvén wave frequencies. In this continuum, the eigenfunctions of the linearized MHD operator are not square integrable due to the existence of spatial singularities, and consequently energy can accumulate without bound at the point of singularity. Among the many effects that can be attributed to this accumulation or equivalently absorption of rf energy, we mention here damping of MHD surface waves. This damping in an inhomgeneous plasma column in MHD has been predicted by several authors (Grad, 1969; Grossmann and Tataronis, 1973), the damping rates calculated for special configurations (Grossmann and Tataronis, 1973) and experimentally verified (Grossmann, Kaufmann and Neuhauser, 1973). The experimental verification of the damping of MHD surface waves was accomplished in a plasma in which one would have expected significant departures from the ideal MHD model, and consequently adds strong support to the assertion that the proposed absorption mechanism is physically real and potentially important. More recently, direct experimental observation of plasma heating by Alfven waves has taken place in several laboratories. Specifically, Golovato, Shohet and Tataronis (1976) have observed heating in the Proto-Cleo Stellarator, while Pochelon and Keller (1977) have observed this heating in a theta pinch. The experimental measurements by Pochelon and Keller are in excellent quantitative agreement with the theoretical predictions of Tataronis and Grossmann (1974, 1976). Other experiments have been carried out by Vo, et al (1976).

The first complete treatment of the theory of resonant absorption in an MHD plasma in the continuous spectrum of stable Alfvén oscillations was given by Tataronis (1975). A special example, i.e., incompressible linearized MHD with spatially varying planar plasma profiles, was examined and the basic underlying theory of the plasma dynamic response to a time varying external source oscillating at frequencies corresponding to the continuum of plasma Alfvén frequencies was given. The results of the theory show that surprisingly good coupling between the source and the plasma can be obtained. The calculations presented in the present paper represent an extension of the theory of Tataronis (1975), and the main new feature of the present work is the complete treatment of currently realistic plasma configurations in cylindrical geometry in a fully compressible ideal MHD model. In particular, we consider reso absorption in such currently interesting plasmas as ST, ORMAK and Scyllac; these plasma configurations are characterized by large magnetic field shear and strong radial inhomogeneity. The calculations thus are made for both low and high-β configurations. One of our goals is to point out that the shape of the plasma profiles plays a major role in the quantitative energy coupling and absorption.

Another feature of the present calculations is that, due to compressibility, a second continuum arises in ideal MHD, and this continuum also results in resonant absorption. The second continuum is conventionally referred to as the cusp continuum and is associated with the singular one-dimensional nature of a

part of the slow magnetoacoustic wave. We show that the cusp continuum indeed yields positive absorption when the external exciting frequency lies in the required frequency range but does not represent a potentially interesting possibility for heating. The reasons are twofold. First, in all cases investigated here the Alfvén continuum yields much stronger absorption and second, the cusp continuum disappears when the guiding center model is used to describe more accurately the plasma (Tataronis and Grossmann, 1976).

Finally, as will become evident later, the numerical results indicate that very strong absorption can be found for practically all types of plasma profiles for exciting frequencies lying in the Alfvén continuum. These results warrant attention since the external apparatus necessary to produce the required energy source is modest.

The remainder of the paper is divided into eleven sections. Section 2 presents the basic equations and mathematical details concerned with the ideal MHD model. In that section, the basic energy integral upon which the absorption theory is based is derived. Section 3 connects the classical folklore of resonant absorption in homogeneous plasmas to that of the present inhomogeneous case. Section 4 considers pertinent characteristics of the solutions to the basic equations. Such features as the singular nature of the eigenmodes and their representation are discussed. Section 5 develops an asymptotic form of the energy absorption rate as a function of the solutions obtained in Section 4. A representation of the effective coil impedance is

developed in Section 6. The actual plasma profiles used are displayed and discussed in Section 7, and numerical techniques employed to solve for the impedance for these profiles are discussed in Section 8. The results of the numerical computations are given in Section 9. Section 10 is devoted to a summary of the experimental work on Alfvén wave heating that has been accomplished to this date. The conclusions of this paper are given in Section 11.

2. Basic Equations

In this section we present the pertinent mathematical details concerning the calculation of the energy absorption. It should be pointed out that the mathematical treatment follows very closely that of Tataronis (1975) and differs primarily in the use of cylindrical coordinates which allow realistic magnetic field shear. A further difference arises in the consideration of fully compressible MHD modes. The plasma-vacuum-source system which we consider is shown schematically in Figure 1. A perfectly conducting diffuse plasma extends to a radius r_p where it is joined to a pure vacuum region. An ideal sheet current is placed at radius r_c, and the entire system is surrounded by a conducting wall at radius r_w.

The Governing Equations

The plasma is described at this point by generalized spatially varying profiles for the magnetic field, pressure and density respectively as:

$$\underset{\sim}{B} = [0, B_\theta(r), B_z(r)] \quad , \tag{1}$$

$$P = P(r) \quad , \tag{2}$$

$$\rho = \rho(r) \quad , \tag{3}$$

where B_θ and B_z are the θ and z components of the equilibrium magnetic field. All quantities vary with the radius r and as $r \to r_p$, $P(r)$ and $\rho(r)$ vanish smoothly. The equilibrium

relationship of ideal MHD connects $P(r)$ and $\underset{\sim}{B}(r)$ through the following equation,

$$\frac{d}{dr}\left(P + \frac{B^2}{2\mu_0}\right) + \frac{B_\theta^2}{r\mu_0} = 0 \ , \tag{4}$$

where μ_0 is the vacuum permeability and B^2 has been written for $B_\theta^2 + B_z^2$. In the vacuum an externally supported, helical surface current is placed at the position $r = r_c$ and is represented as,

$$\underset{\sim}{J}_s(r,\theta,z,t) = [J_{s\theta}(\theta,z,t)\hat{\theta} + J_{sz}(\theta,z,t)\hat{z}]\ \delta(r-r_c) \ , \tag{5}$$

where $\delta(r-r_c)$ is the Dirac delta function and,

$$J_{s\theta} = J_0(t) \cos \nu \cos (m_c\theta + k_c z) \ , \tag{6}$$

$$J_{sz} = J_0(t) \sin \nu \cos (m_c\theta + k_c z) \ , \tag{7}$$

$$\tan \nu = - m_c/k_c r_c \qquad . \tag{8}$$

Here, ν is the pitch angle that the surface current makes with a plane perpendicular to the z-axis as shown in Fig. 1, and J_θ and J_z satisfy the following condition,

$$\frac{m_c}{r_c} J_{s\theta} + k_c J_{sz} = 0 \tag{9}$$

We point out that $\underset{\sim}{J}_s$ has the units of current per unit area, while J_θ and J_z are measured in terms of current per unit length, length being measured in the direction perpendicular to the current density on the surface $r = r_c$. This surface current is the source of the external force which acts on the plasma surface.

Practically, a surface current having helical symmetry can best be approached by line currents which twist around the plasma column, similar to that in the Stellarator configuration. However, due to the discrete nature of such line currents, harmonics of the specified m and k values are generated in the device. Shohet, Golovato and Tataronis (1976) have shown that these harmonics have no adverse effects on the absorption mechanism under consideration here. On the contrary, the harmonics may lead to the desirable condition of local energy absorption at several points across the plasma column.

The plasma dynamics are described by the linearized ideal MHD equations of motion which allow adiabatic compressible displacements. The equations combined with Maxwell's equations reduce to the following set,

$$\rho \frac{\partial \underset{\sim}{v}}{\partial t} = \frac{1}{\mu_0} (\nabla\times\underset{\sim}{B})\times\underset{\sim}{Q} + \frac{1}{\mu_0} (\nabla\times\underset{\sim}{Q})\times\underset{\sim}{B} - \nabla p \ , \tag{10}$$

$$\frac{\partial \underset{\sim}{Q}}{\partial t} = (\underset{\sim}{B}\cdot\nabla)\underset{\sim}{v} - (\underset{\sim}{v}\cdot\nabla)\underset{\sim}{B} - \underset{\sim}{B}\ \nabla\cdot\underset{\sim}{v} \ , \tag{11}$$

$$\frac{\partial p}{\partial t} = - (\underset{\sim}{v}\cdot\nabla)P - \Gamma P\ \nabla\cdot\underset{\sim}{v} \ , \tag{12}$$

where $\underset{\sim}{v}$, $\underset{\sim}{Q}$, p represent the linearized perturbation velocity vector, magnetic field vector and pressure, respectively. The symbol Γ is the ratio of specific heats. All other variables represent previously defined equilibrium quantities.

In the vacuum region the fluctuating perturbed electric, $\delta \underset{\sim}{E}_v$, and magnetic, $\delta \underset{\sim}{B}_v$, fields are determined through,

$$\delta \underset{\sim}{B}_v = \nabla \phi \quad , \tag{13}$$

$$\frac{\partial}{\partial t} \delta \underset{\sim}{B}_v = - \nabla \times \delta \underset{\sim}{E}_v \ , \tag{14}$$

where the magnetic potential ϕ satisfies,

$$\nabla^2 \phi = 0 \ . \tag{15}$$

At $r = r_p$, the plasma and vacuum fields are connected by the usual continuity conditions of ideal MHD which, in linearized form, reduce to,

$$\underset{\sim}{n} \times \delta \underset{\sim}{E}_v = (\underset{\sim}{n} \cdot \underset{\sim}{v}) \underset{\sim}{B}_v \ , \tag{16}$$

$$- \Gamma P \nabla \cdot \underset{\sim}{\xi} + \frac{1}{\mu_0} \underset{\sim}{B} \cdot [\underset{\sim}{Q} + (\underset{\sim}{\xi} \cdot \nabla) \underset{\sim}{B}] = \frac{1}{\mu_0} \underset{\sim}{B}_v \cdot [\delta \underset{\sim}{B}_v + (\underset{\sim}{\xi} \cdot \nabla) \underset{\sim}{B}_v] \ , \tag{17}$$

where $\underset{\sim}{\xi}(\underset{\sim}{r},t)$ is the Lagrangian displacement vector related to $\underset{\sim}{v}$ through,

$$\underset{\sim}{\xi}(\underset{\sim}{r},t) = \int_0^t dt' \ \underset{\sim}{v}(\underset{\sim}{r},t') \ . \tag{18}$$

Equation (16) requires $\underset{\sim}{Q}_v$ to be parallel to the fluctuating plasma-vacuum interface, and eq. (17) requires the jump in total pressure across the fluctuating interface to vanish. The vector $\underset{\sim}{n}$ is the unit vector normal to the interface. The subscript $(\ )_v$ denotes vacuum quantities. Finally, the following jump conditions across the surface current at $r = r_c$ must be satisfied,

$$\underset{\sim}{n} \times [\delta \underset{\sim}{B}_v] = \mu_0 \underset{\sim}{J}_s \ , \tag{19}$$

$$\underset{\sim}{n} \times [\delta \underset{\sim}{E}_v] = 0 \quad , \tag{20}$$

as well as the condition that the perturbed magnetic field be parallel to the metallic wall at $r = r_w$, i.e.,

$$\underset{\sim}{n}\cdot\delta\underset{\sim}{B}_v = 0 \ . \tag{21}$$

Expressed in terms of cylindrical variables, these constraints reduce to the following system:

$r \to 0$:

(i) all dependent variables remain bounded;

$r = r_p$:

(ii)

$$p^* = \frac{1}{\mu_0}\,\underset{\sim}{B}_v\cdot\delta\underset{\sim}{B}_v + \frac{B_\theta^2 - B_v^2}{\mu_0}\,\frac{\xi_r}{r} \tag{22}$$

$$\underset{\sim}{B}\cdot\nabla v_r = \frac{\partial\delta B_{vr}}{\partial t} \tag{23}$$

$r = r_c$:

(iii)

$$[\delta B_{vz}] = -\mu_0 J_{s\theta} \ , \tag{24}$$

$$[\delta B_{vr}] = 0 \qquad ; \tag{25}$$

$r = r_w$:

(iv)

$$\delta B_{vr} = 0 \ . \tag{26}$$

The brackets in the above equations denote the jump in the enclosed quantities in the direction of increasing r.

In a manner similar to that of Tataronis (1975), we make use of the displacement vector $\underset{\sim}{\xi}$ to derive a relationship which expresses the rate of change of the plasma energy in terms of the fields induced by the surface current. The procedure for this derivation involves integrating eqs. (11) and (12) with respect to t, with the initial conditions set equal to zero, substituting the resulting expressions for $\underset{\sim}{Q}$ and p as functions of $\underset{\sim}{\xi}$ into eq. (10), scalar multiplying eq. (10) by $\underset{\sim}{v}$ and then integrating over a plasma region bounded by a surface Σ. The following result is obtained,

$$\frac{dW_p}{dt} = - \oint_{\Sigma} d\underset{\sim}{\sigma} \cdot \underset{\sim}{v}\ p^* \quad , \tag{27}$$

where p^* has been written in place of $p + \underset{\sim}{B} \cdot \underset{\sim}{Q}/\mu_0$, the total perturbed plasma pressure, and W_p represents the sum of the plasma kinetic and potential energies induced by the linearized fields, i.e.,

$$W_p = \frac{1}{2} \int_{V_p} d\tau\ \rho \underset{\sim}{v}^2 + \frac{1}{2} \int_{V_p} d\tau [\frac{1}{\mu_0} \underset{\sim}{Q}^2 + \underset{\sim}{J} \cdot (\underset{\sim}{\xi} \times \underset{\sim}{Q}) + (\nabla \cdot \underset{\sim}{\xi}) \underset{\sim}{\xi} \cdot \nabla P + \Gamma P (\nabla \cdot \underset{\sim}{\xi})^2] \ . \tag{28}$$

Here, V_p is the plasma volume enclosed by Σ. In what follows, V_p will be defined by $r = r_p$, $0 \le \theta \le 2\pi$ and $0 \le z \le L_z$ ($\equiv 2\pi/k_c$) with periodic boundary conditions imposed on the perturbed variables at $z = 0$ and $z = L_z$ as well as at $\theta = 0$ and $\theta = 2\pi$. Equation (27) states that the rate at which the plasma energy increases with time is equal to the energy flux density, $\underset{\sim}{v}p^*$,

directed into the volume integrated over the enclosing surface Σ. If Σ is identical with a plasma-vacuum interface where the boundary conditions given by eqs. (16)-(17) apply, then it is a straightforward matter to express the right-hand side of eq. (27) in terms of the component of the vacuum Poynting vector normal to Σ, which in turn can be related to the time rate of change of the energy associated with the perturbed vacuum magnetic field and to the power delivered by the surface current. For the geometry in Figure 1 and under the assumption that $B_\theta(r)$ varies continuously across the equilibrium plasma-vacuum interface, the following representations of dW_p/dt are readily obtained:

$$\frac{dW_p}{dt} = - \int_0^{2\pi} r_p \, d\theta \int_0^{L_z} dz \; v_r(r_p,t) p^*(r_p,t) \; , \tag{29}$$

$$= - \int_0^{2\pi} r_p \, d\theta \int_0^{L_z} dz \; v_r(r_p,t) \quad \underset{\sim}{B}_v \cdot \delta \underset{\sim}{B}_v(r_p,t) \mu_o^{-1} \; , \tag{30}$$

$$= - \int_0^{2\pi} r_p \, d\theta \int_0^{L_z} dz \; S_r(r_p,t) \; , \tag{31}$$

$$= - \frac{dW_v}{dt} - \int_0^{2\pi} r_c \, d\theta \int_0^{L_z} dz \; \delta \underset{\sim}{E}_v(r_c,t) \cdot \underset{\sim}{J}_S \; , \tag{32}$$

where S_r is the radial component of the vacuum Poynting vector, $\delta \underset{\sim}{E}_v \times \delta \underset{\sim}{B}_v$, and,

$$W_v = \int d\tau_v \, \frac{\delta \underset{\sim}{B}_v^2}{2\mu_0} \; , \tag{33}$$

W_V being the energy of the perturbed vacuum magnetic field and $d\tau_V$ the differential volume element taken in the vacuum.

Equations (10) - (33) form the basis of our investigation. In order to describe the absorption mechanism which is deduced from these equations, it is useful to make use of certain local properties that characterize the linear MHD waves in infinite uniform plasmas. A discussion of these waves is therefore given in the next section where it is shown that two of the three MHD modes imply local motion of the plasma. It is this local motion that is the source of the continuous spectrum of the MHD differential operator and of the resulting energy absorption. In later sections we shall solve eqs. (10)-(12) for $v_r(r,\theta,z,t)$ and $p^*(r,\theta,z,t)$ in terms of the specified surface current and use these solutions to obtain an explicit representation of dW_p/dt through eq. (29). We make use of the resulting expression to derive the experimentally relevant coil impedance and then evaluate this impedance for Tokamak- and Scyllac-like plasmas.

3. Resonances in the Infinite Homogeneous Plasma

In this section we will briefly review MHD wave propagation in infinite, homogeneous plasmas. Specifically, we will connect the classical concepts of resonance and cut-off frequencies in the dispersion characteristics of the MHD waves to the subject of the present paper.

We assume that the equilibrium magnetic field is unidirectional throughout the plasma and that the equilibrium fields do not vary in space. Assuming propagation in the form $\exp i(\omega t - \underset{\sim}{k}\cdot\underset{\sim}{r})$, one can readily derive from eqs. (10)-(12) the following dispersion relation for the linearized MHD waves:

$$(\omega^2-k^2v_a^2\cos^2\theta)[\omega^4-(v_a^2+v_s^2)k^2\omega^2+v_a^2v_s^2k^4\cos^2\theta] = 0 , \quad (34)$$

where k represents the magnitude of the wave vector $\underset{\sim}{k}$, θ is the angle between $\underset{\sim}{k}$ and $\underset{\sim}{B}$, and v_a $(\equiv B/\sqrt{\rho\mu_0})$ and v_s $(\equiv \sqrt{\Gamma P/\rho})$ are respectively the Alfvén and sound speeds. Equation (34) yields three modes of propagation: the Alfvén wave,

$$\omega^2 - k^2v_a^2\cos^2\theta = 0 , \quad (35)$$

and the slow and fast waves,

$$\omega^4 - (v_a^2 + v_s^2)k^2\omega^2 + v_a^2v_s^2k^4\cos^2\theta = 0 . \quad (36)$$

An illuminating representation of the solution of eqs. (35) and

(36) is found in the phase velocity diagram (the Friedrichs diagram) shown in Figure 2, where the loci of ω/k is traced as a function of θ. The envelopes have been drawn assuming $v_s < v_a$. For $v_s < v_a$, the envelope of the Alfvén is tangent to the fast wave envelope at $\theta = 0$. One sees in Fig. 2 that the phase velocity of the fast wave is more or less isotropic in θ but that of the slow and Alfvén waves is highly anisotropic. Of particular importance is the fact that as θ approaches 90°, corresponding to perpendicular propagation, the magnitude of the phase velocity of the slow and Alfvén waves approaches zero. The implication of this property is that localized excitation of the fluid gives rise to perturbations which propagate locally, i.e. free of dispersion in the direction perpendicular to $\underset{\sim}{B}$, about the magnetic line of force on which the initial data was specified. This fact is borne out in Fig. 3 where the wave fronts formed by the three MHD waves excited by a source localized at the origin of an x-z Cartesian coordinate system are plotted at some instant of time. The wave front of the fast wave is isotropic as one would expect, while those of the slow and Alfvén waves are localized to the interior of a cone. The Alfvén wave is actually degenerate in the sense that it has no dispersion. As indicated in Fig. 3, a point disturbance in the Alfvén mode remains a point disturbance localized to the field line on which the excitation was made. Again the Alfvén wave in Fig. 3 represents the case $v_s < v_a$. For $v_s > v_a$, the Alfvén mode is

changed only by moving the point representing the wave front from the slow wave envelope to the fast wave envelope. The slow wave also reveals localization in the form of the vertex of the cusp trailing to the left of the wave front. Considerable effort has been made in the past to investigate the mathematical and physical consequences of the "cusp" motion (Cumberbatch, 1962). The main results are, (1) the cusp origin is a point which moves along the magnetic field line, (2) the cusp motion is a one-dimensional motion, and (3) the speed at which the cusp moves is given by,

$$v_c^2 = \frac{1}{\rho} \frac{\Gamma P \; B^2/\mu_0}{\Gamma P + B^2/\mu_0} \tag{37}$$

The localization of the Alfvén and cusp propagation is the origin of the MHD resonances that we shall refer to later as the cusp and Alfvén wave resonances. In order to bring this resonance phenomenon more in line with the terminology used in plasma wave theory, we show in Fig. 4 the dispersion diagram for the three MHD waves. There, the frequency ω is plotted as a function of $k_\perp$, the component of the wave vector perpendicular to $\underset{\sim}{B}$, with $k_\parallel$, the parallel component, held fixed. In wave theory a resonance is said to occur where the wave vector becomes infinite. In Fig. 4 two such resonances are found. One occurs at $\omega = \omega_a \equiv k_\parallel v_a$; ω_a will be referred to from this point on as the Alfvén frequency. Another such resonance occurs at $\omega = \omega_k \equiv k_\parallel v_k$; ω_k will similarly be referred to as the cusp frequency. One also notices in Fig. 4 that with $k_\parallel$ held fixed, the three MHD waves have cut off

frequencies, i.e. frequencies at which the wave number, $k_{\perp}$ in this case, vanishes.

The importance of resonance and cutoff frequencies arises in connection with the prediction of energy absorption and reflection in spatially inhomogeneous plasmas. Specifically, if one considers an inhomogeneous equilibrium, a differential equation replaces the wave dispersion relationship. The solutions of the differential equation are characterized by singularities which occur in space at the point where the applied frequency equals the local value of the now spatially dependent resonance frequency. Thus, one finds a correspondence between the resonances of an infinite uniform plasma and the spatial singularities of certain macroscopic fluid variables in an inhomogeneous plasma. Depending on the nature of the singularities and the dependence of the wave energy on the perturbed fields, one can establish in certain cases an association between these singularities and unbounded energy at the singular point. Similarly, one can demonstrate a connection between cutoff frequencies in the dispersion characteristics of the homogeneous medium and energy reflection in the inhomogeneous medium. Based on these qualitative ideas, one can now make the following statements in regard to energy absorption in an ideal MHD fluid, namely that energy absorption may be possible at the local Alfvén wave and cusp resonances. In the following sections we shall demonstrate the validity of this assertion. We mention here that other rf plasma heating schemes, such as ion and electron cyclotron heating and lower hybrid

resonance heating, are based on wave resonances of this type.

The above discussion has been concerned with an infinite homogeneous plasma; the main point of the present paper is that it is not only useful but absolutely necessary to consider the inhomogeneous nature of real plasmas in order to treat correctly the absorption of rf energy in a plasma by means of such resonance phenomena. In fact the results which we will later present show that the questions of existence of absorption, the magnitude and the position in the plasma of maximum absorption depend critically on the detailed shape of the inhomogeneous plasma profiles such as those of the pressure, density and magnetic field.

4. Solution of the Equations of Motion

In this section we begin our analysis of the linearized MHD equations in cylindrical geometry. In particular we shall solve eqs. (10) - (12) in the presence of a time varying forcing term and then apply the results to compute the rate at which energy is transferred to the plasma as a result of the action of the forcing term. Moreover we will discuss certain pertinent details of the spectrum of these equations and discuss the nature of solutions in the vicinity of singularities. This information will then be useful in describing the energy absorption processes in the inhomogeneous plasma.

For the present calculation, there is a natural choice of macroscopic variables to use in solving the MHD equations. These variables are the total perturbed pressure p^*, where $p^* = p + \underset{\sim}{Q}\cdot\underset{\sim}{B}/\mu_0$, and the radial perturbation displacement vector ξ_r. These variables occur explicitly in the linearized expressions for the boundary conditions at the vacuum interface. Further, the governing differential equations for these two variables greatly facilitates an investigation of the linearized MHD spectrum as shown by Grad (1974).

We first perform a Laplace transformation with respect to time and a Fourier transform with respect to θ and z by writing,

$$\xi_r(r,\theta,z,t) = \int_L \frac{d\omega}{2\pi} \int_{-\infty}^{\infty} \frac{dk}{2\pi} \sum_{m=-\infty}^{\infty} \exp i(\omega t - m\theta - kz)\ \hat{\xi}_r(r,m,k,\omega),$$
$$\mathrm{Im}\ (\omega) < 0, \qquad (38)$$

where

$$\hat{\xi}_r(r,m,k,\omega) = \int_0^\infty dt \int_{-\infty}^\infty dz \int_0^{2\pi} \frac{d\theta}{2\pi} \exp[-i(\omega t-m\theta-kz)\xi_r(r,\theta,z,t), \tag{39}$$

L being a contour in the complex ω plane below all singularities of the integrand. The other dependent variables are to be treated in an analogous manner. After application of eq. (39), a straightforward manipulation of eqs. (10) - (12) yields the following two differential equations for $\hat{p}^*$ and $\hat{\xi}_r$:

$$\frac{d\hat{p}^*}{dr} = b_0\hat{p}^* + b_1 r\hat{\xi}_r \ , \tag{40}$$

$$\frac{dr\hat{\xi}_r}{dr} = b_2\hat{p}^* - b_0 r\hat{\xi}_r \ , \tag{41}$$

where we have set all initial conditions equal to zero. Equations (40) and (41) can be combined to yield a single second order equation for $\hat{\xi}_r$:

$$\frac{d}{dr}\left[\frac{1}{b_2}\frac{dr\hat{\xi}_r}{dr}\right] - \left[b_1 + \frac{b_0^2}{b_2} - \frac{d}{dr}\left(\frac{b_0}{b_2}\right)\right] r\hat{\xi}_r = 0 \ . \tag{42}$$

The coefficients b_0, b_1 and b_2 are defined as follows. Let,

$$A = -\rho\,\omega^2 + \frac{F^2}{\mu_o} \ , \tag{43}$$

$$C = -(\Gamma P + \frac{B^2}{\mu_0})\omega^2\rho + \Gamma P\frac{F^2}{\mu_0} \ , \tag{44}$$

$$D = \omega^4\rho^2 + (\frac{m^2}{r^2} + k^2)C \ , \tag{45}$$

where as previously defined $B^2 = B_\theta^2 + B_z^2$, and,

$$F = \frac{m}{r} B_\theta + k B_z \quad . \tag{46}$$

The coefficients b_0, b_1 and b_2 then can be written as,

$$\frac{1}{b_2} = - \frac{AC}{rD} \quad , \tag{47}$$

$$b_0 = - \frac{1}{A} \left(2 \frac{B_\theta}{r\mu_0}\right) \left(\frac{m}{r} F + B_\theta \frac{\omega^4 \rho^2}{C}\right) \quad , \tag{48}$$

$$b_1 = + \frac{1}{r} \left[A - 2 \frac{B_\theta}{r\mu_0} r \frac{d}{dr} \left(\frac{B_\theta}{r}\right) - \left(2 \frac{B_\theta}{r\mu_0}\right)^2 \frac{F^2}{A} - \left(2 \frac{B_\theta}{r\mu_0}\right)^2 \frac{\omega^4 \rho^2}{AC} B_\theta^2\right] \tag{49}$$

Equations (40)-(42) have been used by many authors (Grad, 1973; Goedbloed and Sakanaka, 1974) to discuss the MHD spectrum and the normal mode approach to plasma stability of the screw pinch. The absorption process under discussion here depends on the singular nature of the above equations. Specifically, these equations are singular at points $r = r_0(\omega)$ where the coefficients b_0, b_1 or b_2 possess singularities, i.e., at the zeros of $A(r,\omega)$ and $C(r,\omega)$. The factors A and C set equal to zero correspond respectively to the local Alfvén and cusp dispersion relations of the infinite homogeneous plasma considered in Section 3, but written here in terms of cylindrical coordinates. The zeros of A satisfy,

$$\omega^2 = \omega_A^2(r) \equiv \frac{1}{\mu_0} \frac{F^2(r)}{\rho(r)} \quad , \tag{50}$$

while those of C are obtained from,

$$\omega^2 = \omega_C^2(r) \equiv \frac{1}{\mu_0\rho(r)} \quad \frac{\Gamma P(r)F^2(r)}{\Gamma P(r)+B^2(r)/\mu_0} \quad , \tag{51}$$

where ω_A and ω_C are respectively the local frequencies of the Alfvén wave and cusp resonances defined in Section 3. Thus about any $r = r_0(\omega)$ satisfying eqs. (50) or (51), the solutions of eqs. (40) and (41) may be singular. By expanding all coefficients in a power series about the point $r_0(\omega)$, one can prove the existence of a singular solution. One finds in fact the following two linearly independent solutions to eq. (42),

$$f_a = g(r,\omega) \tag{52}$$

$$f_s = g(r,\omega) \ \ln \ (r_0 - r) + (r - r_0) \ h(r,\omega) \quad , \tag{53}$$

where $g(r,\omega)$ and $h(r,\omega)$ are analytic in some domain about r_0, the extent of the domain being determined by the closest other zero of $A(r,\omega)$ or $C(r,\omega)$ to r_0. The general solution for $\hat{\xi}_r$ can thus be written as follows,

$$r\hat{\xi}_r = C_a f_a + C_s f_s \quad , \tag{54}$$

where $C_a(\omega,m,k)$ and $C_s(\omega,m,k)$ are functions independent of r that are determined by invoking boundary conditions at $r = 0$ and $r = r_p$. Hence, for some given ω, the variable ξ_r possesses in general a logarithmic singularity. Actually the singularity manifests itself in a manner stronger than a logarithm. This can be seen in the following manner. Let us first solve for $\hat{\xi}_\theta$

and $\hat{\xi}_z$, the azimuthal and longitudinal components of $\hat{\underset{\sim}{\xi}}$ respectively in terms of $r\hat{\xi}_r$ and $dr\hat{\xi}_r/dr$. A lengthy calculation yields:

$$-\, irD\hat{\xi}_\theta = (-\,\rho\omega^2 E\,\frac{B_z}{\mu_0} + \Gamma P\,\frac{m}{r}\,A)\,\frac{dr\hat{\xi}_r}{dr} + 2\,\frac{B_\theta}{r\mu_0}\,(-\rho\omega^2 B_z + \Gamma PkF)kr\hat{\xi}_r \quad , \tag{55}$$

$$-irD\hat{\xi}_z = (-\,\rho\omega^2 E\,\frac{B_\theta}{\mu_0} + \Gamma PkA)\,\frac{dr\hat{\xi}_r}{dr} - 2\,\frac{B_\theta}{r\mu_0}\,(-\rho\omega^2 B_\theta + \Gamma P\,\frac{m}{k}\,F)kr\hat{\xi}_r \quad , \tag{56}$$

where,

$$E = \frac{m}{r}\,B_z - kB_\theta \quad . \tag{57}$$

The apparent singularity at the zeros of D is misleading, for it can be demonstrated in terms of the solutions for $\hat{\xi}_r$ that $\hat{\xi}_\theta$ and $\hat{\xi}_z$ are analytic at points where D vanishes. By substituting eq. (54) for $\hat{\xi}_r$ in eqs. (55) and (56), one can readily show that about $r_0(\omega)$,

$$\hat{\xi}_\theta \text{ and } \hat{\xi}_z \sim \frac{1}{r-r_0(\omega)} \quad . \tag{58}$$

These variables possess stronger singularities than those of $r\hat{\xi}_r$ in the sense that $\hat{\xi}_\theta$ and $\hat{\xi}_z$ are not square integrable whereas $r\hat{\xi}_r$ is square integrable. As pointed out in the introduction and as will be expanded upon later, the non-square integral singu-

larities of $\hat{\xi}_\theta$ and $\hat{\xi}_z$ form the basis of the energy absorption process which is the subject of the present paper.

In order to proceed with a calculation of the time behavior of ξ_r, it is necessary to consider the coupling of the sheet current to the plasma and determine the singularities of $\hat{\xi}_r(r,\theta,z,\omega)$ in the complex ω plane, where $\hat{\xi}_r(r,\theta,z,\omega)$ is the inverse Fourier transform of $\hat{\xi}_r(r,m,k,\omega)$. The inverse Laplace integral can then be performed on a contour that lies below the singular points. We now briefly describe our construction of $\hat{\xi}_r(r,\theta,z,\omega)$ and then consider in some detail the distribution of the singularities in the complex ω plane. The inversion of the Laplace integral will be considered at the end of this section.

Let us introduce a function $\psi(r,m,k,\omega)$ which is a solution of eq. (42), satisfies the boundary conditions imposed on $\hat{\xi}_r$ at $r = 0$, namely, ψ remain bounded in the limit $r \to 0$, and is normalized by specifying $d\psi/dr$ at $r = 0$. It is clear that these conditions uniquely define ψ which can then be generated by solving eq. (42) as an initial value problem. Except for special equilibrium profiles, ψ must be obtained numerically, We now write,

$$r\hat{\xi}_r(r,m,k,\omega) = R(\omega,m,k)\psi(r,m,k,\omega) \quad , \tag{59}$$

and determine R by invoking the boundary conditions at the plasma-vacuum interface, namely, eqs. (22) and (23). Assuming continuity of B_θ and B_z at $r = r_p$, and expressing δB_v in terms of the magnetic potential Φ through eq. (13), these conditions can be expressed in the following form:

at $r = r_p$

$$\frac{F^2}{r_p} \frac{\hat{\phi}}{d\hat{\phi}/dr} = - \frac{\mu_0}{b_2} \left(\frac{1}{\psi}\frac{d\psi}{dr} + b_0\right) \quad , \tag{60}$$

and,

$$R = - \frac{r_p}{iF\psi} \frac{d\hat{\phi}}{dr} \quad , \tag{61}$$

where Fourier and Laplace transformations have been applied, and $\hat{p}^*$ has been eliminated with eq. (41). We now express the magnetic potential $\hat{\phi}$ in terms of the θ-component of the external surface current by solving Laplace's equation in the vacuum domain subject to the jump and boundary conditions given by eqs. (24)-(26). We give the details of this computation in Appendix A and write the result here as follows:

$$\hat{\phi} = - \operatorname{sgn}(k)\; i\, \mu_0\, r_c\, \hat{J}_{s\theta}\, [I_m(|k|r) - \chi_1 K_m(|k|r)]\chi_2 \quad , \tag{62}$$

where,

$$\chi_1 = \frac{I_m(\tau_p) - |k|q\, I_m'(\tau_p)}{K_m(\tau_p) - |k|q\, K_m'(\tau_p)} \quad , \tag{63}$$

$$\chi_2 = \frac{I_m'(\tau_w)K_m'(\tau_c) - I_m'(\tau_c)K_m'(\tau_w)}{I_m'(\tau_w) - \chi_1 K_m'(\tau_w)} \quad . \tag{64}$$

Here, I_m and K_m are respectively the modified Bessel functions of the first and second kind, the symbol ( )' designates differentiation with respect to the argument of the enclosed function, τ_p, τ_c and τ_w have been written in place of $(|k|r_p)$, $(|k|r_c)$ and $(|k|r_w)$ respectively, k has been taken as real, and q, which is related to the surface impedance at the plasma inter-

face, is defined as follows,

$$q = \frac{\hat{\phi}}{d\hat{\phi}/dr} \quad \text{at} \quad r = r_p \quad . \tag{65}$$

Finally, m is to be interpreted as an absolute value, i.e. as $|m|$. The expression that is to be substituted in eq. (62) for $\hat{J}_{s\theta}$ is the Laplace and Fourier transformations of eq. (6), i.e.,

$$\hat{J}_{s\theta} = \pi \, \hat{J}_0(\omega) \cos \nu \, [\delta_{m,m_c} \delta(k-k_c) + \delta_{m,-m_c} \delta(k+k_c)] \quad , \tag{66}$$

where $\delta_{m,\pm m_c}$ and $\delta(k \pm k_z)$ are respectively the Kroniker and Dirac delta functions. In the analysis below, we shall assume a sinusoidal time dependence for $J_{s\theta}$ at the frequency ω_0, i.e., $J_0(t) = J_0 \sin \omega_0 t$ from which we obtain,

$$\hat{J}_0(\omega) = J_0 \frac{\omega_0}{\omega_0^2 - \omega^2} \quad . \tag{67}$$

At this point, we have sufficient information to construct the pertinent dependent variables in terms of the known function $\psi(r,\theta,k,\omega)$. Equations (60) and (65) are combined to obtain q which in turn is substituted into eq. (63) and (64) to form χ_1, χ_2 and, with eq. (62), $\hat{\phi}$. $\hat{\phi}$ is then substituted in eq. (61) to form R and the result is combined with eq. (59) yielding,

$$r\hat{\xi}_r = \text{sgn}(k) \mu_o r_c \hat{J}_{s\theta}(\omega) \frac{\Delta(\omega)}{F(r_p)} \frac{\psi(r,\omega)}{\psi(r_p,\omega)} \quad , \tag{68}$$

where

$$\Delta(\omega) \equiv \frac{I_m'(\tau_w) K_m'(\tau_c) - I_m'(\tau_c) K_m'(\tau_w)}{I_m'(\tau_w) K_m(\tau_p) - I_m(\tau_p) K_m'(\tau_w) - |k| q(\omega) [I_m'(\tau_w) K_m'(\tau_p) - I_m'(\tau_p) K_m'(\tau_w)]} \quad . \tag{69}$$

The variables $\hat{p}^*$, $\hat{\xi}_\theta$ and $\hat{\xi}_z$ follow by substituting eq. (69) in eqs. (41), (55) and (56) respectively for $r\hat{\xi}_r$.

To obtain ξ_r in the time domain, we first perform an inverse Fourier transformation of eq. (68) with respect to m and k, yielding,

$$r\hat{\xi}_r(r,\theta,z,\omega) = \mu_0 r_c \hat{J}_0(\omega) \frac{\Delta(\omega)}{F(r_p)} \frac{\psi(r,\omega)}{\psi(r_p,\omega)} \cos(m_c\theta+k_c z) \quad , \qquad (70)$$

where eq. (66) was substituted for $\hat{J}_{s\theta}$. In eq. (70), $k \equiv k_c$, $m \equiv m_c$ and $F(r) \equiv (m_c/r_p)B_\theta(r) + k_c B_z(r)$. The time dependence follows by carrying out the inverse Laplace integral of eq. (70) on a contour lying below the singularities of $\hat{\xi}_r(r,\theta,z,\omega)$ in the complex ω plane. The singularities are of two types: poles arising from the zeros of the denominator of $\Delta(\omega)$ and from $\hat{J}_0(\omega)$, and branch points, together with the associated branch cuts, arising from the logarithmic singularities of $\psi(r,\omega)$ about the zeros of $A(r,\omega)$ and $C(r,\omega)$. Details of the branch point singularities can be obtained by making use of the technique employed by Tataronis (1975) whereby in some domain, $r_1<r<r_2$, $\psi(r,\omega)$ is written in the form,

$$\psi(r,\omega) = Q(\omega)[p(\omega)\psi_a(r,\omega) + \psi_s(r,\omega)] \quad , \qquad (71)$$

where $Q(\omega)$ and $p(\omega)$ are functions independent of r, and $\psi_a(r,\omega)$ and $\psi_s(r,\omega)$ are two linearly independent solutions of eq. (42). Recalling that $\psi(r,\omega)$ is obtained by solving eq. (42) as an initial value problem from $r = 0$, we assume that $\psi(r,\omega)$ has been determined up to a point $r = r_1$. $\psi(r,\omega)$ and $d\psi(r,\omega)/dr$ at $r = r_1$ then serve as initial data for the determination of $\psi(r,\omega)$ in a

domain $r_1 < r < r_2$ where we assume that either $A(r,\omega)$ or $C(r,\omega)$ vanish at $r = r_0(\omega)$ for some real ω. We then define $\psi_a(r,\omega)$ as that solution of eq. (42) which is analytic at $r = r_0(\omega)$ and $\psi_s(r,\omega)$ as the singular solution which we can write as,

$$\frac{\psi_s(r,\omega)}{\psi_a(r,\omega)} - \frac{\psi_s(r_1,\omega)}{\psi_a(r_1,\omega)} = \int_{r_1}^{r} \frac{r' D(r',\omega)}{A(r',\omega)C(r',\omega)} \frac{dr'}{\psi_a^2(r',\omega)} \quad . \tag{72}$$

Equation (72) gives $\psi_s(r,\omega)$ in a form whereby the relationship between the zeros of $A(r',\omega)$ and $C(r',\omega)$ i.e. $r_0(\omega)$ and the branch point singularities of $\psi_s(r,\omega)$ in the complex ω plane for a given r is manifestly evident. If $r_0(\omega)$ lies on the real r' axis in the domain $r_1 < r_0(\omega) < r$, then the Cauchy integral on the right hand side of eq. (72) is singular. Changing ω such that $r_0(\omega)$ moves off the r' axis into the complex plane then displaces the singularity of the integrand and permits integration along the real r' axis between r_1 and r. Therefore, contours in the complex ω plane on which $r_0(\omega)$ is real and satisfies $r_1 < r_0(\omega) < r$ are singular lines of the Cauchy integral and hence of $\psi_s(r,\omega)$. Since the coefficients $A(r,\omega)$ and $C(r,\omega)$ are real if ω and r are real, $r_0(\omega)$ can be real only if ω is real, implying that the singular lines of $\psi_s(r,\omega)$ lie on the real ω axis. Typically, for real ω, $r_0(\omega)$ has the form shown in Fig. 5 where the curve in the domain $0 < \omega < (\omega_C)_{max}$ is obtained from $C(r,\omega) = 0$, while for $\omega < (\omega_A)_{min}$, we have $A(r,\omega) = 0$. For $(\omega_C)_{max} < \omega < (\omega_A)_{min}$, neither $C(r,\omega)$ nor $A(r,\omega)$ have real zeros for ω real. If $C(r,\omega)$ and $A(r,\omega)$ are analytic in some domain about the real r axis, then the singular lines of the Cauchy integral are branch cuts. This can be shown

by assuming ω to be complex in eq. (72), $\omega = \omega_r + i\,\omega_i$, and letting ω_i approach zero. One then finds that if $A(r',\omega_r) = 0$ for some real $r' = r_0$, between r_1 and r, $\psi_s(r,\omega)$ is defined on the real ω axis as follows:

$$\frac{\psi_s(r,\omega)}{\psi_a(r,\omega)} - \frac{\psi_s(r_1,\omega)}{\psi_a(r_1,\omega)} = P\int_{r_1}^{r} \frac{r'D(r',\omega)}{A(r',\omega)C(r',\omega)}\,\frac{dr'}{\psi_a^2(r',\omega)}$$

$$+\; i\varepsilon\pi\,\frac{\mathrm{sgn}(\omega)}{\rho(\omega_0)}\,\frac{D(r_0,\omega)}{C(r_0,\omega)}\,\frac{r_0}{\psi_a^2(r_0,\omega)}\left|\frac{d\omega_A^2}{dr}\right|_{r=r_0}^{-1}, \qquad (73)$$

where,

$$\varepsilon \equiv \begin{cases} +1, & \text{if } \omega_i \to 0 \text{ from negative values,} \\ -1, & \text{if } \omega_i \to 0 \text{ from positive values,} \end{cases} \qquad (74)$$

and P designates that the principle value of the integral is to be taken, Therefore, as ω cross the real axis between $\omega_A(r_1)$ and $\omega_A(r)$, $\psi_s(r,\omega)$ encounters a discontinuous jump in value, implying the presence of a branch cut with branch points at $\omega = \omega_A(r_1)$ and $\omega = \omega_A(r)$. Similarly, if $C(r',\omega_r)$ vanishes at $r' = r_0$, one finds the following expression for $\psi_s(r,\omega)$ on the real ω axis,

$$\frac{\psi_s(r,\omega)}{\psi_a(r,\omega)} - \frac{\psi_s(r_1,\omega)}{\psi_a(r_1,\omega)} = P\int_{r_1}^{r} \frac{r'D(r',\omega)}{A(r',\omega)C(r',\omega)}\,\frac{dr'}{\psi_a^2(r',\omega)} \qquad (75)$$

$$+\; i\varepsilon\pi\,\frac{\mathrm{sgn}(\omega)}{[\Gamma P(r_0)+B^2(r_0)/\mu_0]\rho(r_0)}\,\frac{D(r_0,\omega)}{A(r_0,\omega)}\,\frac{r_0}{\psi_a^2(r_0,\omega)}\left|\frac{d\omega_C^2}{dr}\right|_{r=r_0}^{-1}.$$

In deriving eqs. (73) and (75), it has been implicitly assumed

that $d\omega_A^2/dr$ and $d\omega_C^2/dr$ do not vanish at $r = r_0$. If the derivatives of $\omega_A^2(r)$ and $\omega_C^2(r)$ do in fact vanish at $r = r_0$, one would then find that the Cauchy integral has a branch point at $\omega = \omega_A(r_0)$ (Tataronis, 1975). In summary, we show in Fig. 6 the expected branch point and branch line structure of $\psi(r,\omega)$ in the complex ω plane for a given spatial distribution of $\omega_A^2(r')$ or $\omega_C^2(r')$. Designating the resonant frequencies as $\omega_j^2(r')$ with $j \equiv A$ for the Alfvén frequencies and C for the cusp frequency, we assume in Fig. 6a a form of $\omega_j^2(r')$ which has $d\omega_j^2/dr' = 0$ at $r' = 0$, r_1 and r_2. As indicated in Fig. 6b, branch points are therefore expected at $\omega = \omega_j(0)$, $\pm\, \omega_j(r_1)$, $\pm\, \omega_j(r_2)$ and at $\omega = \pm\, \omega_j(r)$.

We are now in a position to carry out the inverse Laplace transform of $r\hat{\xi}_r(r,\theta,z,\omega)$ to obtain $r\xi_r(r,\theta,z,t)$. Combining eqs. (39) and (70) and assuming eq. (67) for $\hat{J}_0(\omega)$, we find, after deforming the contour L to a contour L' which encircles the singularities of the Laplace integrand and extends into the upper half ω-plane, the following expression,

$$r\xi_r(r,t) = J_0 R_\xi(r,\omega_0)\sin\omega_0 t + J_0 X_\xi(r,\omega_0)\cos\omega_0 t + \eta(r,t) \quad , \tag{76}$$

where R_ξ and X_ξ are respectively the real and imaginary parts of the complex function Z_ξ, i.e.,

$$Z_\xi(r,\omega) \equiv R_\xi(r,\omega) + iX(r,\omega) \quad , \tag{77}$$

with

$$Z_\xi(r,\omega) \equiv r\hat{\xi}_r(r,\omega)/\hat{J}_0(\omega) \quad . \tag{78}$$

From eq. (70), we obtain,

$$Z_\xi(r,\omega) = \mu_0 r_c \frac{\Delta(\omega)}{F(r_p)} \frac{\psi(r,\omega)}{\psi(r_p,\omega)} \quad , \tag{79}$$

where the factor $\cos(m_c\theta + k_c z)$ has been dropped for convenience of notation. The θ and z dependence of $r\xi_r$ is then simply given in terms of eq. (76) as,

$$r\xi_r(r,\theta,z,t) = r\xi_r(r,t)\cos(m_c\theta+k_c z) \quad . \tag{80}$$

The term $\eta(r,t)$ is eq. (76) represents the transient part of the plasma response to the applied external force, and is given by,

$$\eta(r,t) = \int_{L'} \frac{d\omega}{2\pi} \exp(i\omega t) Z_\xi(r,\omega)\hat{J}_\theta(\omega) \tag{81}$$

where the deformed contour L' encloses only the singularities of the kernal $Z_\xi(r,\omega)$, the simple poles of $\hat{J}_\theta(\omega)$ having already been accounted for through the first two terms in the right hand side of eq. (76). The singularities consist of the branch points and branch cuts of $\psi(r,\omega)$ and of the poles of $\Delta(\omega)$. For the profile shown in Fig. 6a, this would then lead to the contour L' given in Fig. 7 where the branch cuts have been analytically continued off the real ω axis into the complex plane. The poles indicated in Fig. 7 are zeros of the denominator of $\Delta(\omega)$, i.e., they satisfy

$$I'_m(\tau_w)K_m(\tau_p) - I_m(\tau_p)K'_m(\tau_w) - |k|q(\omega)[I'_m(\tau_w)K'_m(\tau_p) - I'_m(\tau_p)K'_m(\tau_w)] = 0 \quad . \tag{82}$$

The poles at $\omega = \omega_m^\alpha$, ω_m^β, ω_m^γ are the magnetoacoustic modes which

depend on the compressibility of the plasma. For the incompressible plasma, these discrete modes are absent. The complex poles at $\omega = \omega_s^\alpha$, ω_s^β are damped surfaces oscillations, discussed in detail elsewhere (Grossmann and Tataronis, 1973; Tataronis, 1975), which appear explicitly in the response only if the branch cuts are analytically continued into the upper half plane as in Fig. 7. In general these roots of eq. (82) are complex, and the implied decay originates from phase mixing of the Alfven and cusp continuum modes.

Although the integration of eq. (81) along L' cannot be carried out explicitly, one can obtain an asymptotic expression for $\eta(r,t)$ as $t \to \infty$. The result is,

$$\eta(r,t) \underset{\sim}{\sim} \alpha(r) \frac{\cos\omega_j(r)t}{\omega_j(r)t} + \sum_\nu \gamma_\nu(r) \frac{\cos\omega_\nu t}{(\omega_\nu t)^{\eta_\nu}}$$

$$+ \sum_\alpha S_\alpha(r)\exp(-\omega_{si}^\alpha t)\cos\omega_{sr}^\alpha t$$

$$+ \sum_\beta T_\beta(r)\cos\omega_m^\beta t \quad . \qquad (83)$$

where ω_{sr}^α and ω_{si}^α are the real and imaginary parts of ω_s^α respectively. The first two terms in the right hand side of eq. (83) decay in time and arise from integration about the branch points in Fig. 7. The third term is the decaying surface oscillation and the last term represents the steady magnetoacoustic modes.

Our main interest of course lies in regions about $r = r_0$ where $\omega_0^2 = \omega_A^2(r_0)$ or $\omega_C^2(r_0)$. Here the singularities of $\Xi_\xi(\omega)$

$\hat{J}_\theta(\omega)$ interact to yield higher order singularities. For both an Alfvén $[\omega_0 = \omega_A(r_0)]$ and a cusp $[\omega_0 = \omega_C(r_0)]$ type resonance the singularity is of the form:

$$r\hat{\xi}_r(r,\omega) \sim \frac{\ln(\omega - \omega_0)}{\omega - \omega_0} \quad , \tag{84}$$

which implies,

$$r\xi_r(r,t) \sim \ln t \cos \omega_0 t \quad , \tag{85}$$

asymptotically as $t \to \infty$. Thus $r\xi_r(r,t)$ grows logarithmically with time at the point $r = r_0$. From eqs. (55) and (56) it can be shown that $\xi_\theta(r,t)$ and $\xi_z(r,t)$ at the point $r = r_0$ behave temporally as follows:

$$\xi_\theta(r,t) \sim \xi_z(r,t) \sim t \cos \omega_0 t \quad . \tag{86}$$

It is this local temporal growth at r_0 which will be associated with local energy absorption at that point. In the next section we will use the above solutions in an asymptotic calculation of energy absorption for $t \to \infty$.

5. Asymptotic Form of Energy Absorption

In this section we will consider the time behavior of the plasma energy W_p in the limit as $t \to \infty$. We will average dW_p/dt over a period of the given frequency of the external source. If this average is greater than zero, then it can be concluded that the plasma absorbs energy. Alternatively, one can obtain the average rate of change of the plasma energy by calculating the average rate at which energy is delivered by the external source. Because of eq. (27) which expresses conservation of energy, the average loss or gain of energy by the source should equal respectively the average gain or loss of energy by the plasma. This equality will be established in Section 6.

First we specialize the general form of W_p, the total perturbed plasma energy, given by eq. (28), for the specific case of cylindrical symmetry. Assuming periodic boundary conditions in both θ and z, a lengthy calculation yields,

$$
\begin{aligned}
\frac{dW_p}{dt} = \frac{d}{dt} \int d\tau \Bigg[& \frac{1}{2}\rho_0 (v_r^2+v_\theta^2+v_z^2) + \frac{1}{2\mu_0}\left\{(\underset{\sim}{B}\cdot\nabla\xi_r)^2+(\underset{\sim}{B}\cdot\nabla\xi_\theta)^2+(\underset{\sim}{B}\cdot\nabla\xi_z)^2\right\} \\
& + \frac{1}{2}\left(\Gamma P + \frac{B^2}{\mu_0}\right)(\nabla\cdot\underset{\sim}{\xi})^2 - \frac{1}{2\mu_0 r}\left(\frac{B_\theta^2}{r^2}\right)' r^2\xi_r^2 - \frac{1}{\mu_0}\left(\underset{\sim}{B}\cdot\nabla(\underset{\sim}{B}\cdot\underset{\sim}{\xi}) + \frac{2B_\theta^2}{r^2} r\xi_r\right)\nabla\cdot\underset{\sim}{\xi} \\
& + \frac{2B_\theta}{\mu_0 r}\xi_r\, \underset{\sim}{B}\cdot\nabla\xi_\theta \Bigg] \quad , \qquad (87)
\end{aligned}
$$

where ( )' denotes differentiation with respect to r. The volume element $d\tau \equiv r\,dr\,d\theta\,dz$ with $0 \leq r \leq r_p$, $0 \leq \theta \leq 2\pi$ and $0 \leq z \leq 2\pi/k_c$. In eq. (87) we denote by δKE the first three terms, the perturbed kinetic energy of the plasma. The remaining terms

we will denote by δW, the perturbed potential energy. In the following we shall make use of the identity:

$$\int_0^{2\pi} d\theta \int_0^{2\pi/k_c} dz \begin{cases} \cos^2(m_c\theta+k_c z) \\ \sin^2(m_c\theta+k_c z) \end{cases} = \pi\lambda \ , \ \lambda = \frac{2\pi}{k_c} \ . \tag{88}$$

The integrands of δKE and δW are functions of r, m_c and k_c. We have seen that at the point $r = r_0$ where either A or C vanishes, singularities of the Laplace transform of the fluctuating variables exist with the consequence that these variables grow with time at r_0 upon application of a harmonic force. At every other point, the perturbation fields saturate in amplitude as $t \to \infty$. Therefore, for t large, the major contribution to the kinetic and potential energies arises from some narrow region of width Δr about the point r_0. We express this as:

$$\delta KE = \frac{\pi\lambda}{2} \int_{r_0-\Delta r}^{r_0+\Delta r} r \, dr \, \rho \underset{\sim}{v}^2 + \delta(\delta KE) \quad , \tag{89}$$

$$\delta W = \frac{\pi\lambda}{2} \int_{r_0-\Delta r}^{r_0+\Delta r} r \, dr \left[\frac{\underset{\sim}{Q}^2}{\mu_0} + \underset{\sim}{Q}\cdot(\underset{\sim}{J}\times\underset{\sim}{\xi}) + \nabla\cdot\underset{\sim}{\xi}(\xi_r P' + \Gamma P \nabla\cdot\underset{\sim}{\xi}) \right] + \delta(\delta W) \tag{90}$$

Using here again, the general form of eq. (28), section 2. The terms $\delta(\delta KE)$ and $\delta(\delta W)$ result from the remaining parts of the spatial integration. As $t \to \infty$, $d\delta(\delta KE)/dt$ and $d\delta(\delta W)/dt \to 0$. Therefore in computing the time rate of change of the energy $\delta(\delta KE)$ and $\delta(\delta W)$ can be neglected. Considering the solutions found in the last section we notice that the fastest growing fields and variables at a singular point r_0 are v_θ, v_z , ξ_θ , ξ_z ,

Q_θ , Q_z for both the Alfvén and the cusp mode with the exception that $\nabla\cdot\xi$ must be included for the cusp singularity. In the following we treat the Alfvén and cusp absorption separately.

<u>Alfvén Absorption</u>

At the point r_0 where $\omega_0^2 = \omega_A^2(r_0)$, the function $A(r_0,\omega)$ vanishes, and it can be shown that Q_θ , Q_z , ξ_θ , ξ_z , v_θ and v_z are related accordingly,

$$Q_\theta = F\,\xi_\theta \ , \tag{91}$$

$$Q_z = F\,\xi_z \ , \tag{92}$$

$$\underset{\sim}{Q}^2 = F^2(\xi_\theta^2 + \xi_z^2) \ , \tag{93}$$

$$\underset{\sim}{v}^2 = v_\theta^2 + v_z^2 = \omega_A^2(r_0)\,(\xi_\theta^2 + \xi_z^2) \ , \tag{94}$$

where the definition $\underset{\sim}{v} = \partial\underset{\sim}{\xi}/\partial t$ has been used in eq. (94). Consequently, the form of δKE and δW reduce to the following expressions,

$$\delta KE \approx \frac{\pi\lambda r_0}{2} \int_{r_0-\Delta r}^{r_0+\Delta r} dr\ \rho \underset{\sim}{v}^2 \ , \tag{95}$$

$$\delta W \approx \frac{\pi\lambda r_0}{2} \int_{r_0-\Delta r}^{r_0+\Delta r} dr\ \frac{\underset{\sim}{Q}^2}{\mu_0} \ , \tag{96}$$

where for clarity we have neglected $\delta(\delta KE)$ and $\delta(\delta W)$. Substituting eq. (93) into eq. (96) we obtain an expression for the lowest order total perturbed plasma energy about the singular point,

$$\delta KE + \delta W \simeq \frac{\pi\lambda r_0}{2}\,\rho(r_0)\int_{r_0-\Delta r}^{r_0+\Delta r} dr\left[v_\theta^2 + v_z^2 + \omega_A^2(r_0)(\xi_\theta^2+\xi_z^2)\right] \quad , \tag{97}$$

where $\omega_A^2(r_0) \equiv F^2(r_0)/\rho(r_0)\mu_0$. In order to proceed it is necessary to obtain the variables $v_\theta(r,\omega)$, $v_z(r,\omega)$, $\xi_\theta(r,\omega)$ and $\xi_z(r,\omega)$ about the point r_0. This can be readily accomplished since the form of $r\hat{\xi}_r(r,\omega)$ at this point is known and is given by eq. (84). Using eqs. (55) and (56) we can define $\hat{\xi}_\theta$ and $\hat{\xi}_z$ in terms of $r\hat{\xi}_r$ and $(r\hat{\xi}_r)'$; the inverse Laplace transform may be accomplished with the result in the limit $t \to \infty$,

$$\xi_\theta^2(r,t) + \xi_z^2(r,t) = J_\theta^2\,\frac{R_\theta^2+R_z^2}{4\omega_0^4}\cos^2(\omega_0 t+\phi_\theta)\,\frac{\sin^2[\frac{1}{2}\,\omega_A'(r_0)(r-r_0)t]}{[\frac{1}{2}\,\omega_A'(r_0)(r-r_0)]^2} \quad , \tag{98}$$

and

$$v_\theta^2(r,t) + v_z^2(r,t) = J_\theta^2\,\frac{R_\theta^2+R_z^2}{4\omega_0^2}\sin^2(\omega_0 t+\phi_\theta)\,\frac{\sin^2[\frac{1}{2}\,\omega_A'(r_0)(r-r_0)t]}{[\frac{1}{2}\,\omega_A'(r_0)(r-r_0)]^2} \quad , \tag{99}$$

where R_θ and R_z are constants which are specified by applying boundary conditions at the plasma vacuum interface in the same manner in which $C(\omega)$ was determined for the function $r\hat{\xi}_r(r,\omega)$ through eq. (60). Using eqs. (98) and (99) we can express the total energy as,

$$\delta KE + \delta W \approx$$

$$\frac{\pi\lambda r_0}{2}\,\rho(r_0)\omega_A^2(r_0)\;J_\theta^2\,\frac{R_\theta^2+R_z^2}{4\omega_0^2}\int_{r_0-\Delta r}^{r_0+\Delta r} dr\,\frac{\sin^2[\frac{1}{2}\,\omega_A'(r_0)(r-r_0)t]}{[\frac{1}{2}\,\omega_A'(r_0)(r-r_0)]^2} \quad , \tag{100}$$

$$\simeq \frac{\pi\lambda r_0}{2} J_\theta^2 \frac{R_\theta^2+R_z^2}{\omega_0^2} \frac{2\pi t}{|\omega_A'(r_0)|} \tag{101}$$

Applying the boundary conditions on ξ_θ and ξ_z through the corresponding boundary conditions for $r\xi_r$ yields the result:

$$R_\theta^2+R_z^2 = \left[\frac{F^4}{\mu_0^2} \frac{B^2E^2}{\mu_0^2} \frac{1}{r_0^2D^2}\right]_{r_0} \frac{\mu_0^2\omega_0^2}{F^2(r_p)} \frac{r_c^2[K_m'(\tau_c)]^2}{|K_m(\tau_p) - kqK_m'(\tau_p)|^2} \times \frac{[(\omega_A^2(r_0))']^2}{|\psi(r_p)|^2} , \tag{102}$$

where

$$D(r_0) = -\frac{F^2(r_0)}{\mu_0} \frac{E^2(r_0)}{\mu_0} \tag{103}$$

and in the above, for the purpose of clarity, the wall radius r_w has been removed to infinity. Substitution of eq. (102) into eq. (101) yields the final result for the temporal behavior of the total perturbed plasma energy in the singular layer,

$$\delta KE + \delta W \simeq \frac{\pi\lambda r_c^2 J_\theta^2}{4r_0} \left(\pi\omega_0^2 t\right) \frac{B^2(r_0)}{E^2(r_0)} \frac{\mu_0^2}{F^2(r_p)} \rho(r_0) \times \frac{[K_m'(\tau_c)]^2}{|K_m(\tau_p) - kq\, K_m'(\tau_p)|^2} \frac{|(\omega_A^2(r_0))'|}{|\psi(r_p)|^2} \tag{104}$$

We now differentiate (104) with respect to time to obtain the power supplied to the plasma and average this expression over one period, T_0, of the external source, $T_0 = 2\pi/\omega_0$, to obtain

$$\langle P\rangle_{T_0} = \frac{\pi\lambda r_c^2}{2r_0} J_\theta^2\omega_0 \frac{B^2(r_0)}{E^2(r_0)} \frac{\mu_0^2\rho(r_0)}{F^2(r_p)}$$

$$\times \frac{[K_m'(\tau_c)]^2}{|K_m(\tau_p) - kqK_m'(\tau_p)|^2} \frac{|(\omega_A^2(r_0))'|^2}{|\psi(r_p)|^2} \tag{105}$$

Equation (105) is a positive definite quantity representing the energy absorbed by the plasma in a narrow region about the point r_0 where the external frequencey of the source ω_0 equals the local Alfvén frequency of the plasma $\omega_A^2(r_0)$.

Cusp Absorption

We now consider the case when $\omega_0^2 = \omega_C^2(r_0)$. The procedure here is identical to that for the Alfvén mode. As mentioned earlier, the fastest growing fields at the point r_0 where C vanishes are Q_θ , Q_z , v_θ , v_z , ξ_θ , ξ_z and $\nabla\cdot\vec{\xi}$. The divergence term, $\nabla\cdot\vec{\xi}$, reflects the fact that the cusp mode only occurs when compressibility is included in the equations of motion. Again using the relationships between ξ_θ , ξ_z and $r\xi_r$ it can be shown that where $C(r_0)$ vanishes,

$$Q_\theta \cong F\xi_\theta - B_\theta\nabla\cdot\underset{\sim}{\xi} , \tag{106}$$

$$Q_z \cong F\xi_z - B_z\nabla\cdot\underset{\sim}{\xi} . \tag{107}$$

The divergence $\nabla\cdot\underset{\sim}{\xi}$ can similarly be treated and at r_0 can be shown to be

$$\nabla\cdot\underset{\sim}{\xi} = -\frac{A(r_0)}{r_0\rho(r_0)\omega^2} \frac{d}{dr} r\xi_r . \tag{108}$$

The form of the total perturbed energy for the cusp mode is given in a similar manner to that of the Alfvén mode, i.e., we consider again only the contribution arising from some narrow region of width $2\Delta r$ about the resonance or singular point r_0 and neglect the contributions from the remainder of the integration. We have then for the cusp mode:

$$\delta KE = \frac{\pi\lambda r_0}{2} \int_{r_0-\Delta r}^{r_0+\Delta r} dr\ \rho(r)\ [v_\theta^2(r) + v_z^2(r)]\ , \tag{109}$$

$$\delta W = \frac{\pi\lambda r_0}{2} \int_{r_0-\Delta r}^{r_0+\Delta r} dr \left[\frac{Q_\theta^2(r)}{\mu_0} + \frac{Q_z^2(r)}{\mu_0} + \Gamma P(r)(\nabla\cdot\underset{\sim}{\xi})^2\right] . \tag{110}$$

We now form the products Q_θ^2 and Q_z^2 ,

$$Q_\theta^2 = F^2\xi_\theta^2 + B_\theta^2(\nabla\cdot\underset{\sim}{\xi})^2 - 2B_\theta F\xi_\theta\ \nabla\cdot\underset{\sim}{\xi}\ , \tag{111}$$

$$Q_z^2 = F^2\xi_z^2 + B_z^2(\nabla\cdot\underset{\sim}{\xi})^2 - 2B_z F\xi_z\ \nabla\cdot\underset{\sim}{\xi}\ , \tag{112}$$

such that,

$$Q_\theta^2 + Q_z^2 = F^2(\xi_\theta^2+\xi_z^2) + B^2(\nabla\cdot\underset{\sim}{\xi})^2 - 2F\underset{\sim}{B}\cdot\underset{\sim}{\xi}\ \nabla\cdot\underset{\sim}{\xi}\quad . \tag{113}$$

Using once more the relationship between ξ_θ, ξ_z and $r\xi_r$ we find at the point r_0 where $C(r_0) = 0$,

$$\xi_\theta \cong \frac{1}{rD}\left(-\Gamma PA\frac{m}{r} + \rho\omega^2 E\frac{B_z}{\mu_0}\right)\frac{d}{dr}\,r\xi_r \tag{114}$$

$$\xi_z \cong \frac{1}{rD}\left(\Gamma PAk + \rho\omega^2 E\frac{B_\theta}{\mu_0}\right)\frac{d}{dr}\,r\xi_r \tag{115}$$

where

$$D(r_0) \simeq \rho^2\omega^4 \quad . \tag{116}$$

Expanding the numerators of eqs. (114) and (115) leads to the simpler expressions,

$$- \Gamma PAm/r + \rho\omega^2 B_z E/\mu_0 = - \rho\omega^2 \frac{B_\theta F}{\mu_0} \tag{117}$$

$$\Gamma PAk + \rho\omega^2 B_\theta E/\mu_0 = \rho\omega^2 \frac{B_z F}{\mu_0} \tag{118}$$

Hence, the form of ξ_θ and ξ_z can be conveniently written as,

$$\xi_\theta \simeq - \frac{B_\theta F}{\mu_0 r\rho\omega^2} \frac{d}{dr} r\xi_r \ , \tag{119}$$

$$\xi_z \simeq - \frac{B_z F}{\mu_0 r\rho\omega^2} \frac{d}{dr} r\xi_r \ , \tag{120}$$

from which we obtain,

$$\underset{\sim}{B}\cdot\underset{\sim}{\xi} \simeq - \frac{(B_\theta^2+B_z^2)F}{\mu_0 r\rho\omega^2} \frac{d}{dr} r\xi_r \tag{121}$$

An expression for $\xi_\theta^2+\xi_z^2$ can now be obtained as,

$$\xi_\theta^2 + \xi_z^2 \quad \frac{B^2F^2}{r^2\mu_0^2\rho^2\omega^4} \left(\frac{d}{dr} r\xi_r\right)^2 \tag{122}$$

from which the following is obtained

$$(\underset{\sim}{B}\cdot\xi)F \ \nabla\cdot\underset{\sim}{\xi} \approx \frac{(B_\theta^2+B_z^2)F^2A}{r^2\mu_0^2\rho^2\omega^4} \left(\frac{d}{dr} r\xi_r\right)^2 \ , \tag{123}$$

$$F^2(\xi_\theta^2+\xi_z^2) \approx \frac{B^2F^4}{r^2\mu_0^2\rho^2\omega^4} \left(\frac{d}{dr} r\xi_r\right)^2 \quad . \tag{124}$$

It is convenient to consider the terms δKE and δW separately; we begin with δW. So far we have obtained the following form for δW,

$$\delta W = \frac{\pi\lambda r_0}{2} \int_{r_0-\Delta r}^{r_0+\Delta r} dr \left[\frac{B^2F^4}{r^2\mu_0^3\rho^2\omega^4} + \frac{(\Gamma P+B^2/\mu_0)A^2}{r^2\rho^2\omega^4} - \frac{2B^2F^2A^2}{\mu_0^2\rho^2\omega^4 r^2}\right]\left(\frac{d}{dr}\, r\xi_r\right)^2 \tag{125}$$

which is equivalent to,

$$\delta W = \frac{\pi\lambda}{2r_0}\left(\frac{B^2F^4}{\mu_0^3} + (\Gamma P + \frac{B^2}{\mu_0})A^2 - \frac{2B^2F^2A^2}{\mu_0^2}\right)\frac{1}{\rho^2\omega^4}\int_{r_0-\Delta r}^{r_0+\Delta r} dr\left(\frac{d}{dr}\, r\xi_r\right)^2 \tag{126}$$

A computation of the inverse Laplace transform of $dr\hat{\xi}_r/dr$ yields the result,

$$\frac{d}{dr}\, r\xi_r(t) \approx -\frac{J_\theta}{2\omega_0^2}\,|\tilde{R}(\omega_0)|\; 2\cos(\omega_0 t+\phi)\,\frac{\sin[\frac{1}{2}\,\omega_C'(r_0)(r-r_0)t]}{[\omega_C'(r_0)(r-r_0)]}\;, \tag{127}$$

where $\tilde{R}(\omega_0)$ is a constant which will be specified later. The integral in eq. (126) can thus be carried out to give the result

$$\int_{r_0-\Delta r}^{r_0+\Delta r} dr\left(\frac{d}{dr}\, r\xi_r\right)^2 = \frac{J_\theta^2}{\omega_0^4}\,|\tilde{R}(\omega_0)|^2\,\frac{\cos^2(\omega_0 t+\phi)\pi t}{|(\omega_C^2(r_0))'|}\;. \tag{128}$$

An evaluation of boundary conditions at the plasma-vacuum interface allows $\tilde{R}(\omega_0)$ to be specified. The result is,

$$|\tilde{R}(\omega_0)|^2 = \frac{\mu_0^2\omega_0^2 r_c^2}{F^2(r_p)}\,\frac{[K_m'(\tau_c)]^2}{|K_m(\tau_p) - kqK_m'(\tau_p)|^2}\,\frac{[(\omega_C^2(r_0))']^2}{|\psi_a+i\psi_s|^2}\;, \tag{129}$$

where again for clarity the wall position, $r = r_w$, has been taken to be at infinity. Expanding the coefficient before the integral in eq. (126) yields a simpler expression which when combined with the result of the integration yields the final form for δW

$$\delta W \approx \frac{\pi\lambda r_0}{2} \left(\frac{B^2F^2}{\mu_0^2\rho^2\omega_0^4 r^2}\right)_{r=r_0} \frac{J_\theta^2|\tilde{R}(\omega_0)|^2}{\omega_0} \frac{\pi t \cos^2(\omega_0 t+\phi)}{|(\omega_C^2(r_0))'|} \tag{130}$$

The calculation of the kinetic energy proceeds in a similar manner. We first express v_θ and v_z as functions of t through the relations given by eqs. (55) and (56). The result is

$$v_\theta(t) = \frac{B_\theta F}{r_0\mu_0\rho\omega_0^2} J_\theta \frac{|\tilde{R}(\omega_0)|}{2\omega_0} 2 \sin(\omega_0 t+\phi) \frac{\sin[\frac{1}{2}\omega_C'(r_0)(r-r_0)t]}{[\omega_C'(r_0)(r-r_0)]} \tag{131}$$

and

$$v_z(t) = -\frac{B_z F}{r_0\mu_0\rho\omega_0^2} J_\theta \frac{|\tilde{R}(\omega_0)|}{2\omega_0} 2 \sin(\omega_0 t+\phi) \frac{\sin[\frac{1}{2}\omega_C'(r_0)(r-r_0)t]}{[\omega_C'(r_0)(r-r_0)]} \tag{132}$$

where we have retained only the parts which lead to growth in δKE at $r = r_0$. Collecting results, the expression for δKE at this point can be written as,

$$\delta KE = \frac{\pi\lambda r_0}{2} \rho(r_0) \left(\frac{B^2F^2}{\mu_0^2\rho^2\omega_0^4 r^2}\right)_{r=r_0} J_\theta^2 \frac{|\tilde{R}(\omega_0)|^2}{4\omega_0^4} \sin^2(\omega_0 t+\phi)$$
$$\int_{r_0-\Delta r}^{r_0+\Delta r} dr \frac{\sin^2[\frac{1}{2}\omega_C'(r_0)(r-r_0)t]}{[\frac{1}{2}\omega_C'(r_0)(r-r_0)]^2} , \tag{133}$$

which integrates to yield,

$$\delta KE = \frac{\pi\lambda r_0}{2}\ \rho(r_0)\left(\frac{B^2F^2}{\mu_0^2\rho^2\omega_0^4 r^2}\right)_{r=r_0} J_\theta^2\ \frac{|\tilde{R}(\omega_0)|^2}{\omega_0}$$

$$\times\ \sin^2\ (\omega_0 t + \phi)\ \frac{\pi\ t}{|(\omega_C^2(r_0))'|}\ . \tag{134}$$

If we now add δKE to δW we obtain the final result for the total perturbed plasma energy,

$$\delta KE + \delta W \cong \frac{\pi^2\lambda r_c^2}{2}\ \omega_0 t\mu_0\ J_\theta^2\ \frac{B^2(r_0)}{r_0 E^2(r_p)}\left(\frac{\omega_A}{\omega_C}\right)^2_{r_0}\ \frac{|(\omega_C^2(r_0))'|}{\omega_C^2}$$

$$\times\ \frac{[K_m'(\tau_c)]^2}{|K_m(\tau_p) - kqK_m'(\tau_p)|^2}\ \frac{1}{|\psi(r_p)|^2}\ , \tag{135}$$

where here $\omega_A^2 = (F^2/\rho\mu_0)_{r=r_0}$. Taking the derivative with respect to time of eq. (135) gives the following result for the power supplied to the plasma,

$$\langle P\rangle_{T_0} = \frac{\pi^2\lambda r_c^2}{2}\ \omega_0\mu_0 J_\theta^2\ \frac{B_\theta^2(r_0)}{r_0 E^2(r_p)}\left(\frac{\omega_A}{\omega_C}\right)^2\ \frac{|(\omega_C^2(r_0))'|}{\omega_C^2}$$

$$\times\ \frac{[K_m'(\tau_c)]^2}{|K_m(\tau_p) - kqK_m'(\tau_p)|^2}\ \frac{1}{|\psi(r_p)|^2}\ . \tag{136}$$

Equation (136) is a positive quantity, and we interpret this as a demonstration that energy emanating from an external source may be absorbed by the plasma at a point r_0 where the external exciting frequency ω_0 equals the local cusp frequency $\omega_C(r_0)$.

We have now demonstrated that it is possible through wave resonance phenomena at the local Alfvén and cusp frequencies in an inhomogeneous plasma column to couple energy from an external source to the plasma in the resonance layers.

Even though the expressions for the absorbed power are convincing, a more useful quantity for the purposes of numerical computations is the effective coil impedance which is felt by the source due to the presence of the plasma. In the next section we calculate this impedance and use it later for numerical investigations of energy absorption in several realistic plasma configurations.

6. Coil Impedance

A very useful and measurable quantity which indicates the amount of absorbed and circulating energy in a system which is excited by an external coil is the coil impedance. Usually the impedance is complex, the real part indicating absorption (or in classical systems dissipative damping), and the imaginary part representing the fraction of the total energy circulating in the system. We will see that the average charge of the plasma energy $\langle dW_p/dt \rangle$ as computed with the resistive part of the coil impedance is identical with the results of Section 5 where $\langle dW_p/dt \rangle$ is computed directly. The current in the idealized coil which we have chosen flows on the coil surface. We begin the calculation of the impedance by noting that the time-averaged power absorbed by the plasma is obtained from eq. (32) and is given by the real part of,

$$\bar{P} = -\frac{1}{2}\pi L_z r_c \, \delta \underset{\sim}{E} \cdot \underset{\sim}{J}_s^{\star} , \qquad (137)$$

where $\bar{P}$ is the absorbed power, δE, as defined before, is the perturbation electric field at the coil and $\underset{\sim}{J}^{\star}$ is the complex conjugate of the total coil current which has components in the θ and z directions, as given by eq. (5). Use of Maxwell's equation plus eq. (9) allows $\delta \underset{\sim}{E} \cdot J_s^{\star}$ to be written as

$$\delta \underset{\sim}{E} \cdot \underset{\sim}{J}_s^{\star} = -\frac{\omega}{k} \delta B_{vr} \, J_{s\theta}^{\star} , \qquad (138)$$

and hence the total time-averaged power as,

$$\bar{P} = \frac{1}{2}\pi L_z r_c \frac{\omega}{k} \delta B_{vr} \, J_{s\theta}^{\star} . \qquad (139)$$

δB_{vr} is derived from the magnetic potential ϕ where $\delta \underset{\sim}{B} = \nabla\phi$ and ϕ is given by eq. (A8) in the Appendix. Computing δB_r as $\partial\phi/\partial r$ and substituting into eq. (139) yields the following equation for the average power $\bar{P}$,

$$\bar{P} = - i\omega\mu_0 \frac{\pi r_c}{2} \frac{r_c}{r_p} \frac{\chi_2(\omega)}{\Delta(\omega)} |J_{s\theta}|^2 \tag{140}$$

where $\chi_2(\omega)$ and $\Delta(\omega)$ are given by eqs. (64) and (70b) respectively. In eq. (140) k and m are respectively equal to m_c and $(-k_c)$. From this expression we can define an impedance $Z(\omega)$ given by:

$$\bar{P} = \frac{1}{2} Z(\omega) |J_{s\theta}|^2 , \tag{141}$$

where

$$Z(\omega) = - i\omega\mu_0 \pi r_c \frac{r_c}{r_p} \frac{\chi_2(\omega)}{\Delta(\omega)} \tag{142}$$

$Z(\omega)$ will have both real and imaginary parts if q is complex. The value of q is obtained from knowledge of the radial component ξ_r at the plasma boundary. Calculation of ξ_r and the subsequent value of q is discussed later. It is clear however that in the absence of singularities in the Alfvén or cusp continuum, ξ_r is a real quantity resulting in a real value for q, and hence the impedance $Z(\omega)$ will be purely imaginary. This would imply no absorption and the total power in the system would be circulatory. We point out that the real part of eq. (141) is identically equal to eq. (105) in the Alfvén continuum.and to eq. (136) in the cusp continuum. Therefore, the absorbed energy implied by the real part of $Z(\omega)$ is transferred to the local resonances of ideal MHD.

7. The Plasma Profiles

We present here the actual plasma profiles which have been used to calculate the absorption. As shown by Tataronis (1975) the quantitative absorption rate depends sensitively on the functional shape of the continuum of Alfvén frequencies inside the plasma column. This means that although positive absorption can be found for any plasma, significant differences may be noticed between several different plasma configurations. By using realistic profiles we are assured that any peculiar characteristics of real experimental plasmas are taken into account. For our calculations we have chosen both Tokamak and Scyllac profiles. The profiles have been assembled through available experimental data and in some cases best guesses averaged over several experiments. It should be pointed out here that the profiles have been adjusted to exclude effects of toroidicity since the present calculations are carried out for straight cylindrical geometry.

Details of the experimental measurements are not discussed here. The first case presented here is the Princeton ST Tokamak. This plasma is basically a low-β plasma with the equilibrium being given mainly by the poloidal magnetic field. The functional form for the various profiles are given below:

$$B_z(r) = B_0 = \text{const.} \,, \tag{143}$$

$$\rho(r) = \rho_0[1 - (r/R_p)^4] , \tag{144}$$

$$J_z(r) = \frac{32\ I_z}{6\pi^2 r_p^2} \left\{1 - (r/r_p)^4\right\}^{3/2} \tag{145}$$

$$rB_\theta(r) = \frac{4\mu_0 I_z}{6\pi^2} \left[\left\{1 - (\frac{r}{r_p})^4\right\}^{3/2} (\frac{r}{r_p})^2 + \left\{\frac{3}{2} \left(1 - (\frac{r}{r_p})^4\right)^{1/2} (\frac{r}{r_p})^2 + \sin^{-1}(\frac{r}{r_p})^2\right\}\right] . \tag{146}$$

In the above ρ_0 is the density on the axis, I_z is the total longitudinal (toroidal) current in amperes, r_p the plasma radius. Equation evaluated at the plasma radius yields,

$$B_\theta(r_p) = \frac{\mu_0 I_z}{2\pi r_p} . \tag{147}$$

The equilibrium relationship, eq. (4), gives the radial pressure variation as:

$$P(r) = \frac{\mu^2 B_0^2}{\mu_0} \left[\frac{1-f_\theta^2}{2} + \int_0^1 \frac{f_\theta(x')^2\ dx'}{x'} - \int_0^x \frac{f_\theta(x')^2\ dx'}{x'}\right] , \tag{148}$$

where $f_\theta = B_\theta(r)/(\mu B_0)$ and the parameter μ is the ratio of the poloidal to the longitudinal magnetic field at the plasma radius, i.e.,

$$\mu = \frac{\mu_0 I_z}{2\pi r_p B_0} . \tag{149}$$

In eq. (148), $x = r/r_p$. For these profiles the limit of P/ρ as $r \to r_p$ yields zero. At the plasma radius $r = r_p$, vacuum profiles for B_θ are joined, and P and ρ are identically zero. The following table contains values of the constants in the above formulas obtained from the experimental data of the ST Tokamak (Hosea, 1974):

Parameters of the ST Tokamak

$$B_0 = 12 - 45 \text{ k Gauss}$$
$$\rho_0 = 2 \times 10^{13} \text{ /cm}^3$$
$$I_z = 10 - 100 \text{ k amperes}$$
$$r_p = 12 \text{ cm}$$

The distribution of Alfvén frequencies in the plasma column is calculated from the following equation after the parameters "m" and "k" have been chosen:

$$\tilde{\omega}_A^2 = \frac{1}{\tilde{\rho}(r)} \left[\frac{m}{x} \mu f_\theta(x) + \tilde{k}\right]^2 , \tag{150}$$

where $\tilde{\omega}_A$ is the frequency normalized according to:

$$\tilde{\omega} = \frac{\omega r_p}{v_a} , \qquad v_a = \frac{B_0}{\sqrt{\mu_0 \rho_0}} , \quad \text{and} \quad \tilde{k} = kr_p .$$

Similarly, the cusp frequency is given by the expression,

$$\tilde{\omega}_c^2 = \frac{\Gamma\tilde{P}}{(\Gamma\tilde{P}+1+\mu^2 f_\theta^2)} \left(\frac{m}{x} \mu f_\theta + \tilde{k}\right)^2 , \tag{151}$$

where $\tilde{P}$ is the normalized pressure, $(P/B_0^2/\mu_0)$. Figure 8 presents the radial dependence of the profiles of $\tilde{B}_z$, f_θ , $\tilde{P}$ and $\tilde{\rho}$ from the axis to the plasma radius. Figure 9 shows the radial dependence of $\tilde{\omega}_A$ and $\tilde{\omega}_c$. The value of μ used for Figures 8 and 9 has been set equal to 0.05. The values of m and $\tilde{k}$ are 1 and 1.1 respectively. The value of k corresponds to a 60 cm wavelength. Near the edges of the plasma the Alfvén continuum tends to large frequency values whereas the cusp

continuum goes to zero. This is a consequence of the limit of $\tilde{P}/\tilde{\rho}$ tending to zero. From Figure 9 one sees a continuous range of frequencies from zero to infinity with the exception of the strip $\tilde{\omega}_{c\ max} \leq \omega \leq \tilde{\omega}_{A\ min}$. It is readily seen that by adjusting the "m" and "$\tilde{k}$" for a given profile this strip can be made as small as possible.

The second set of profiles investigated are those from the ORMAK experiment at Oak Ridge National Laboratory. These profiles correspond to two operating regimes of the experiment, the so-called "A" and "B" type of discharges. It will be convenient to present these profiles in the following manner. Let $\tilde{\mathcal{F}}(r)$ denote a particular radial profile and consider $\tilde{\mathcal{F}}(r)$ to be given by the following function:

$$\tilde{\mathcal{F}}(r) = \tilde{\mathcal{F}}(0)\left(1 - (r/r_p)^n\right)^m , \tag{152}$$

where $\tilde{\mathcal{F}}(0)$ represents the function evaluated on the axis. The following table (England, 1975) then gives the values of n, m and $\tilde{\mathcal{F}}(0)$ for the cases treated here.

Parametres of the ORMAK Tokamak

$\tilde{\mathcal{F}}(r)$	Discharge Type	n	m	$\tilde{\mathcal{F}}(0)$
$\rho(r)$	A	2	2	$4 \times 10^{13}/cm^3$
	B	2	2	$3 \times 10^{13}/cm^3$
$J_z(r)$	A	1.5	1	$133\ amp/cm^2$
	B	4	3	$125\ amp/cm^2$

The plasma radius is 23 cm and the main longitudinal magnetic field was 18 k Gauss. Again, here the longitudinal magnetic field is constant and the poloidal field is computed from Ampere's law as before. The pressure is given by eq. (148) once the poloidal field is known. Although we do not show them, curves similar to those of Figure 9 can be obtained from the Ormak profiles. Although similar, the shapes are different; this difference being a key factor in the actual values of computed absorption.

In an attempt to connect the parameters "k" and μ with experimental configurations, let us form the following dimensionless number kr_p/μ. If the true toroidal plasma had a circumference of length $L = 2\pi R_T$ where R_T is the major torus radius, then,

$$\frac{kr_p}{\mu} \equiv \frac{2\pi n}{L} \frac{B_z(r_p)}{B_\theta(r_p)} r_p = n \frac{B_0 r_p}{B_\theta(r_p) R_T} = nq(r_p) \ , \tag{153}$$

where n is the number of wave lengths along the cylinder of length L and $q(r_p)$ is the well known safety factor evaluated at the limiter. Typically, for the range of parameters examined in this work, the value of q at the plasma radius (limiter in the experiment) was 3 and n corresponds to the order of about 10 wave lengths.

We turn next to the high-β Scyllac profiles. Although the Scyllac experiment is basically a helically toroidal, large aspect ratio ($R_T/r_p >> 1$) plasma configuration, the main magnetic field component is the θ-pinch field. All other fields are of a much smaller order. For this reason we will approximate the

Scyllac plasma by a θ-pinch. We mention only briefly that the existing Scyllac feedback stabilization system could be effectively used to investigate the Alfvén wave absorption (assuming stable plasmas with sufficient life times can be obtained). Here there is only one field component, the axial field, and we use as an approximation the following function:

$$B_z(r) = -(B_0 - B_i)[(r/r_p)^4 - 2(r/r_p)^2] + B_i \ , \tag{154}$$

for $0 \le r \le r_p$, and,

$$B_z = B_0 \quad \text{for} \quad r > r_p \ . \tag{155}$$

B_0 is the constant B_z field in the vacuum and B_i is the value of B_z at $r = 0$. The standard definition of β is thus,

$$\beta = \left[1 - (B_i/B_0)^2\right]^{1/2} .$$

From eq. (4) the pressure is found as,

$$P = \frac{B_0^2}{2\mu_0}\left(1 - \frac{B_z^2}{B_0^2}\right) \tag{156}$$

For the density, a Gaussian profile adjusted to zero density at $r = r_p$ and further adjusted for an appropriate half width consistent with the above equilibrium is chosen. Typically the magnetic field strength B_0 was taken as 40 k Gauss, the density on axis to be $3 \times 10^{16}/cm^3$, the plasma radius 2.5 cm and the wall radius 5 - 10 cm. The value of β can be varied from zero to unity. Figure 10 shows the radial variation of the equilibrium quantities. The Alfvén and cusp continuum frequencies are shown in Figure 11

for the choice $m = 1$ and $\tilde{k} = 0.4$. The value of β as shown in the curves was taken to be $\beta = 0.5$ on the plasma axis.

We mention that the profile given in eq. (155) for the B_z field can be used to construct reversed field conditions such as those produced in a reverse bias θ-pinch experiment. For this situation the β definition must be altered to,

$$\beta = \frac{P_{max}}{B_0^2/2\mu_0} , \tag{157}$$

where P_{max} is the value of the pressure at the point where the B_z field reverses. For a $\beta = 0.5$ we show in Figure 12 the Alfvén and cusp continuum again for $m = 1$ and $k = 0.4$. Notice that it is now possible to find multiple points in the plasma where the applied frequency equals a local Alfvén or cusp frequency. It has been conjectured that such profiles lead to enhanced absorption (Tataronis, 1974). The plasma produced in the Garching poloidal belt-pinch experiment is an example of such a configuration.

We next discuss certain numerical techniques used in applying these profiles to the energy absorption formulation.

8. Numerical Techniques

In this section the pertinent numerical techniques used in obtaining the final value of the coil impedance are discussed briefly. As shown in Section 6, the impedance calculation requires the value of the quantity $(r\xi_r)'/(r\xi_r)$ evaluated at the plasma-vacuum interface. This quantity is obtained as follows. The governing equations (40) and (41) for $r\xi_r$ and p_1^* respectively are expanded about the origin to give starting conditions for the numerical integration of these two equations. A convenient normalization specifies the initial data. From the origin up to the position in radius where the first Alfven or cusp singularity occurs, the solutions for $r\xi_r$ and p_1^* are purely real. The treatment of the solutions about singularities are handled by defining a small region of width 2ε about the singular point. The differential equations defining $r\xi_r$ and p_1^* are integrated numerically up to the point $r_0-\varepsilon$, where r_0 denotes the singular point. These solutions are then continued anaytically to the other side of the singularity at $r = r_0+\varepsilon$ by means of a power series expansion of the solution as given by eqs. (52) and (53). Specifically we invoke for ω real the following analytic continuation,

$$r\xi_r = \begin{cases} \alpha_1(\omega)[\alpha_2(\omega)g(r,\omega)+g(r,\omega)\ \ln(r_0-r)+(r-r_0)h(r,\omega)], & r<r_0, \quad (158) \\ \alpha_1(\omega)[(\alpha_2\underline{+}i\pi)g(r,\omega) + g(r,\omega)\ \ln(r-r_0)+(r-r_0)h(r,\omega)], & r>r_0, \quad (159) \end{cases}$$

where the constants $\alpha_1(\omega)$ and $\alpha_2(\omega)$ are determined by assuming continuity of $r\xi_r$ and $dr\xi_r/dr$ at $r = r_0-\varepsilon$, and the sign of i

in eq. (159) is uniquely determined by invoking causality in the form of the limiting process $\mathrm{Im}(\omega) \to 0$ from the lower half of the complex ω plane. At $r = r_0+\varepsilon$, the values of $r\xi_r$ and p_1^* serve as initial data in order to continue the numerical integration to $r = r_p$. Up to the position of the first singularity, the solutions are purely real. Continuation past the singularity with eq. (159) results in an imaginary part from the logarithm, and therefore the solutions will be complex at $r = r_p$. At this point the value of q, eqs. (60) and (65), can be calculated and hence the absorption rate. The dependence of the value of q on the width of the region 2ε was investigated by varying both the numerical size of ε and the number of terms in the series expansions for $r\xi_r$ and p_1^* about the singular points. Both ε and the number of terms were varied until convergence on q was obtained.

One special case must be mentioned. It is possible that for certain profiles at a given frequency, the position of a singular point may fall very close to a zero of the fast and slow magneto-acoustic branch. When two such points identically coincide the singularity disappears (the strength is reduced from $\ln(x-x_0)$ to $(x-x_0)\ln(x-x_0)$). A problem in the numerical treatment of such a small separation of singularity and zero arises due to the occurrence of large gradients in the region between the points. This can be eliminated by using an inner and outer expansion about the singularity and zero respectively and analytically continuing past the mutual region where both expansions are valid. For the cases treated by us, such problems only occurred for frequencies in the cusp continuum.

All numerical work was carried out on the New York University, Courant Institute CDC 6600 Computer. Typically a computation of the impedance for one frequency, one wavelength and "m" value requires about one second.

9. Numerical Results

In this section we present the results of numerical computation of the effective coil impedance for the profiles specified in Section 7. The pertinent numerical details concerning the integration of the equations of motion (40) and (41) have already been given in Section 8. We begin with a discussion of the ST Tokamak plasma.

The available frequency range for both the Alfvén and cusp bands can be computed from eqs. (150) and (151). From Figure 9 an indication can be obtained as to the position where the maximum absorption for the Alfvén waves occur . This is true since the power absorbed is directly proportional to $|(\omega_A^2(r))'|$ at the resonance point as shown by eq. (104). From Figure 9 it can be seen that strong absorption should only occur at radial positions greater than at least 60% of the plasma radius. This will be shown to actually be the case as borne out by the numerical results. Figure 13 presents the results of the numerical computations of the real part of the coil impedance, Z_R , versus the frequency f. Both Z_R and f are given in dimensional form, ohms and cycles per second respectively. The first noticeable result is the fact that the cusp impedance values are very small, typically less than about 0.02 ohms over the cusp frequency range. For this reason they are not shown plotted in the figure. The Alfvén resistance however is plotted. The values for the, admittedly very ideal case, are

impressively large. Here the ratio of coil radius to plasma radius is 1.5 and the wall has been taken at infinity. We will discuss in detail later the important effect of the conducting wall. Shown in the figure are the results for both an $m = 1$ and $m = 2$ coil. The effect of changing m for the ST plasma is seen to be rather slight, the main effect being a shift in the position of maximum absorption. For the ST data the absorption curves rise sharply to a maximum and then fall gradually; the range of frequency for strong absorption is rather broad. No attempt was made to try to maximize the impedance by varying the coil wave length; the value was chosen to be 60 cm and corresponds to about 10 wave lengths around the actual toroidal plasma. It is also noticed that the absorption falls to zero at isolated values of frequency. Analysis of this behavior shows that the vanishing of the resistance at isolated frequencies arises if the solution of the MHD equations are simultaneously analytic at the Alfven resonance and consistent with the boundary condition at $r = 0$. One then concludes that the logarithm appearing in eq. (53) is absent, implying that ξ_r and q are real, and hence that Z is imaginary. An inspection of $\xi_r(r)$ for ω in the neighborhood where the phenomenon occurs shows that ξ_r oscillates in r, with one-half period of spatial oscillation entering the domain between $r = 0$ and the singular point at each crossing of a critical ω. These oscillations probably correspond to the excitation of the fast MHD wave which propagates in toward the center of the plasma column where it is reflected to form a standing wave.

Let us turn now to the profiles which model the Ormak plasma. This configuration is again a Tokamak plasma but as pointed out above the operation can be one of two types, type A and B discharges. Our intention here is not to discuss the nature of these two types of discharges but to use only the data resulting from them. For the Ormak plasma, both A and B type discharges, the same results for the cusp absorption are found as in the case of the ST plasma. The coil impedances are very low, typically .01 - .1 ohms. The values of impedance for the Alfvén mode however are very large again and as shown in Figure 14, also for a rather ideal case where the coil now is assumed to be right at the plasma edge, can be as much as 50 Ω. The results shown in Figure 14 are for a type A discharge and the wall has again been taken to infinity. We notice some difference from the ST plasma in that the form of the curves for $m = 1,2,3$ show more qualitative differences. The calculations were not carried far enough to obtain the maximum for $m = 2$ and $m = 3$. The normalized wave number, $\tilde{k}$, for the coil was fixed at .287. No interaction with stable kink modes was found for this case. If we now consider the type B profiles with all other parameters held fixed, Figure 15, we obtain once again strong evidence that the spatial variation of the plasma profiles plays an important role in the actual energy absorption. The effect of changing the coil wave length may be seen in Figure 16 where the same parameters and profiles of Figure 15 were assumed but with a coil of exactly one-half the wavelength. Here it can be seen that the wave length also plays an important role in

the energy absorption. Again no effect was made to obtain an optimum in the absorption rate with respect to the coil wave length.

At this point it is appropriate to discuss the effect of an externally conducting wall. Here, we will consider only a perfectly conducting wall. The position of the wall may be an important consideration for the present day and next generation Tokamak experiments for the following reason. It is desirable to create a plasma with the largest possible cross-section inside magnetic field coils; the plasma column must of course be surrounded by a vacuum vessel. The space between the edge of the plasma column and the vacuum vessel may thus be very small. Consequently any coil placed between the plasma column and the outer liner or vacuum vessel could suffer from the effects of mirror currents induced in the outer wall. Of course if the outer wall were constructed in a segmented manner preventing long current paths, this problem would be minimized. We have performed a series of calculations using the Ormak "A" profiles in which it has been assumed that a conducting wall surrounds the coil and have varied the wall position from a distance of say 10 cm to a few cm away from the coil. Figure 17a shows the results from these calculations; shown is the real impedance versus frequency for the case where the coil is assumed to be placed at the edge of the plasma and the wall position varied from $r_w/r_p = 10$ to $r_w/r_p = 1.1$. As expected the impedance decreases drastically as the wall is brought near the coil. Noticeable also is the effect of shifting the position of maximum

absorption to higher frequencies the closer the wall is to the coil. Shown in Figure 17b are the values of the imaginary part of the coil impedance from which along with the real part of impedance, the effective "Q" of the plasma-coil-wall system may be calculated. It can be seen that by dividing the imaginary by the real impedance, "Q" values of from 3-6 in the low frequency range are obtained. Such values allow the classification of such a system as a "low-Q" system suggesting efficient use of energy in the external circuit. If we now move the coil away from the edge of the plasma and simultaneously vary the wall position we obtain the results shown in Figure 18. Here the position of the coil $r_c/r_p = 1.5$, and again the wall position is varied from $r_w/r_c = 10$ to $r_w/r_c = 1.1$. Shown in Figure 18a is the real impedance versus frequency and characteristic decrease of impedance as the wall is brought closer to the coil. For this case it is seen that the position in frequency of maximum absorption varies only slightly as the wall is brought closer to the coil. Figure 18b shows the corresponding computed values of the imaginary part of the impedance and again low "Q" values are obtained. It is thus recognized that it is desirable to have ample space between coil and wall in order to insure reasonable power absorption. Looking towards the future reactor geometries it can be seen that the problem of the external wall can be minimized or perhaps even neglected. This is due to the possibility of the use of a diverter which would necessitate a larger external vacuum region in which coil structures could be

placed. These considerations are not the subject of the present paper, and we leave them to later investigations.

Finally let us consider the results for the high-β configuration described earlier. We consider the β value on plasma axis to be .5 and consider an $m = 1$ coil structure. This choice would correspond to an $\ell = 1$ system in the actual helical Scyllac configuration. The wave length for the coil has been taken to be equal to the helical wave length in the present Scyllac device, and the coil position $r_c/r_p = 1.5$. We neglect here the effect of the external wall. The results of the calculation of the real impedance versus frequency are shown in Figure 19. Here, the cusp absorption rate shows a marked increase over and above that for the previous Tokamak configurations with maximum values of the order of one ohm or so. The Alfvén absorption rate, however, again dominates as seen in the figure and leads to very impressive predictions concerning the coupling of energy to the plasma. Here also, a calculation of the effective "Q" value for the system defines the process to be a "low-Q" system with values typically between 3-6 at maximum absorption.

We have thus demonstrated numerically that effective coupling of energy from an external source can be accomplished through the MHD resonances. Coupling is possible in both the Alfvén mode dominating for typical Tokamak and Scyllac plasma profiles.

10. Experimental Verification of Alfvén Wave Heating

In this section, we consider recent and past experimental investigations aimed at confirming various aspects of the theory of Alfvén wave damping, absorption and heating. It will be shown that there is ample evidence to confirm the theory set forth in this report; there exists close quantitative comparison between theoretical prediction and experimental measurements. In order, we will outline results from the ISAR I helical theta-pinch experiment (Garching), the Proto Cleo Stellarator experiment (Wisconsin), the Heliotron D. Experiment (Kyoto), and a very recent linear theta-pinch experiment (Lausanne).

The first full experimental verification which yielded a confirmation of the fundamental principles upon which the theory of resonant Alfvén wave heating is based was performed in the ISAR I helical theta-pinch at Garching. This experiment consisted of a 5.4 meter long theta-pinch coil whose inner surface was machined to produce an $\ell = 1$ helical magnetic field component. The implosion phase of the plasma column formation followed a more or less normal theta-pinch like form with the helical perturbation being felt at a somewhat later time. This delay resulted in a standing $\ell = 1$ helical oscillation of the plasma column. The mode structure of the column could be described as basically an m = 1 long wavelength perturbation. The wavenumber of the perturbation was equal to that of the helical field component, $K \equiv 2\pi/\lambda_H$, where λ_H is the wavelength of the helical field. This helical perturbation was observed to oscillate at approximately the Alfvén frequency ω_A computed as

$$\omega_A^2 = (2-\beta)(kV_A)^2 \tag{160}$$

(the Alfvén speed V_A was calculated from the density inside the plasma column and the main magnetic field outside the plasma column). Further, the helical oscillation was observed to damp away after two to three oscillation peridos. This damping was several orders of magnitude larger than that which could be expected to occur from purely classical effects such as resistivity and viscosity. The experimentally deduced damping decrements were compared with theoretical calculations (Tataronis and Grossmann, Grossmann and Tataronis, 1973) for a wide range of plasma parameters which covered both collision dominated and collisionless regimes. We show below a sample of the results from the Garching investigation (Grossmann, Kaufmann, Neuhauser, 1973).

T_i	$n(10^{16}cm^{-3})$	$(\gamma/\omega_A)_{EXP}$	$\omega_{ci}\tau_{ii}$	$(\gamma/\omega_A)_{CLASSICAL}$	$(\gamma/\omega_A)_{THEORY}$
25	8	0.2	0.25	3×10^{-4}	
50	4	0.15	1	2×10^{-3}	$\gtrsim 0.2$
100	2	0.1	3.5	10^{-3}	
300	2	0.1	40	5×10^{-5}	

In the above table, the values of ion temperature T_i, plasma density n are given at the time of maximum magnetic field. The experimental values of γ divided by ω_A were approximately constant over the entire regime from the collisional phase ($\omega_{ci}\tau_{ii}$ = .25) to the collisionless regime ($\omega_{ci}\tau_{ii}$ = 40) where ω_{ci} is the ion

cyclotron frequency and τ_{ii} is the ion-ion collision time. It is noticed that the values of $(\gamma/\omega_A)_{CLASSICAL}$ are many orders of magnitude less than the experimental values. The theoretical predictions for the damping assuming a simple form for the inhomogeneous plasma profiles can be seen to agree well with the experimental ones. These results are felt to give conclusive proof that the experimentally observed damped helical Alfvén oscillations are surface waves which decay due to phase mixing (Tataronis and Grossmann, Grossmann and Tataronis, 1973).

The next experiment we consider was performed in the proto-cleo stellarator at Wisconsin (Golovato, Shohet, and Tataronis, 1976). Proto-cleo is a $\ell = 3$ stellarator with seven field periods in the toroidal direction. The aspect ratio of the plasma is between 8 and 9, a reasonable number for a cylindrical approximation to the torus. Alfvén wave heating was produced with a separate electrostatically shielded helical winding whose pitch was designed to approximate a $q = 3$ rational magnetic surface. According to measured magnetic field and density profiles for the proto-cleo plasma, for a constant frequency of the externally applied rf source, two Alfvén resonance regions were predicted at minor plasma radii of approximately 1.5 and 3.5 cm. During the course of the experiment, the resonant regions vary in position according to changes in plasma density profiles. It was experimentally shown that the incident Alfvén wave amplitude did not decrease in the plasma region; this implies that the wave penetrated into the plasma. Shown below are the results of a local measurement of the electron temperature with rf compared to that without

rf as a function of the plasma minor radius. It is noticed that a peaking of the ratio of T_e with rf to T_e without rf occurred near the region of the expected Alfvén wave resonance.

Minor radius	$\frac{T_e \text{ with rf}}{T_e \text{ without rf}}$
0	1.0
0.5	1.5
1.0	1.25
1.5	1.75
2.0	1.25
2.5	1.75
3.0	2.0
3.5	1.5
4.0	1.25
4.5	1.0

The variation of energy absorption and heating with external frequency was consistent with the calculations of heating efficiency for proto-cleo according to theoretical predictions (Tataronis and Grossmann, 1976). The temperature of both electrons and ions increased by a factor of two during heating and this heating was global in nature since the coil structure surrounded the entire plasma.

The next experiment we consider was performed on the heliotron D machine at Kyoto (Uo et al, 1976). This device is basically an $\ell = 2$ plasma with a large rotational transform and strong magnetic shear. The aspect ration for this plasma is, similar to proto-cleo, about 8. A local $\ell = 2$-like coil structure was used to

couple external rf power into the Alfvén resonances of the plasma column. Similar results to those of proto-cleo were observed in the heliotron D device. That is, in the regions where the resonances were predicted to occur both ion and electron temperatures, were significantly increased (ion and electron temperatures were approximately doubled). It was further shown that the coil loading resistance was high implying that the coupling corresponds to low-Q and broad resonance. This is consistent with theoretical predictions (Tataronis and Grossmann, 1976). The heating efficiency was estimated to be as large as 60%.

Finally we consider results from an Alfvén wave heating experiment on a high-β linear theta pinch plasma column (Pochelin, Keller, 1977). In this experiment a rather dramatic confirmation of Alfvén wave heating was observed. The basic experiment consists of a 1.4 meter linear theta pinch plasma with mean density $\sim 1.3 \times 10^{16}$ cm^{-3}, total temperature $\sim$ 50 eV, and mean plasma beta $\sim$ 0.25. A helical excitation winding giving an $m = 1$ perturbation with approximately two full wavelengths was applied to the plasma column. The application of the helical perturbation field took place approximately 1.5μs after the main magnetic field had been turned on; this allowed enough time for the natural or magnetoacoustic oscillations to have damped away. It was noticed in the experiment that when the exciting coil was driven continuously, that the plasma helical motion was less damped at frequencies below the Alfvén wave resonance peak (corresponding to the surface wave resonance); above this resonance point, the helical plasma motion was damped rapidly. When the coil was

operated with only two excitation periods and at resonance the kink-like helical motion is more strongly absorbed than at lower frequency. After the excitation was shut off, the unforced plasma motion showed nearly critical damping in complete agreement with theoretical predictions (Tataronis and Grossmann, Grossmann and Tataronis, 1973). From a knowledge of the time evolution of the plasma radius and diamagnetic probe measurements, the mean value of the total plasma temperature was deduced. The plasma temperature was raised on the order of 15 to 20% during the short heating pulse and it was further ascertained that approximately 50% of the excitation power was thermalized in the plasma. This number also corresponds to a coupling efficiency of approximately 50% and consequently shows the method to be very attractive for heating. The measured power absorbed by the plasma as a function of the coil frequency follows a curve which is identical to that shown in Fig. 19.

11. Conclusions

A complete, self-consistent and rigorous treatment of rf energy absorption through the use of the linearized MHD equations of motion in inhomogeneous plasmas by means of Alfvén waves has been presented. A model system is considered consisting of a straight cylindrically symmetric plasma column surrounded by a vacuum region in which an idealized coil is placed. The plasma profiles are inhomogeneous in the direction perpendicular to the cylinder axis and the entire plasma-vacuum-coil system is surrounded by a conducting wall. It has been shown that rf energy can be irreversibly absorbed by the plasma when the external coil is oscillated at frequencies which lie in the Alfvén continuous frequency spectrum given by the nonuniform plasma profiles. The resonant absorption mechanism is discussed in complete detail and the following general results have been found: (i) strong absorption is predicted at reasonably low frequencies independent of the plasma total β ; (ii) variations in plasma profiles are refelcted in significant differences in total absorption and in the spatial position of maximum absorption; (iii) the position of the coil and external wall relative to the plasma column plays an important role in the rf absorption. Calculations with realistic Tokamak and Scyllac plasma profiles have been carried out to illustrate the above; values of the effective coil impedance as a function of coil and plasma parameters have been computed. From the numerical results it can be shown that the Alfvén wave heating scheme

is a low "Q" technique (Q = ratio of circulating to absorbed power) and should because of the inherent low frequencies and long wave lengths be considered for a supplementary heating technique on future large plasma containment devices.

It is worth noting that recent calculations on resistive (Kappraff, Tataronis, Grossmann, 1975; Kappraff,and Tataronis, 1977) and kinetic (Hasegawa and Chen, 1975; Gould, 1975; Thompson, 1975) effects have indicated that the energy transferred to the resonant Alfvén region in the plasma is converted rapidly to electron thermal energy.

Finally, in support of the above remarks, we mention that experimental evidence, in particular from the proto-cleo and Lausanne θ-pinch experiments, has been obtained to substantiate the claim that rf energy can be coupled efficiently to an inhomogeneous plasma column through the continuous spectrum of stable Alfvén plasma oscillations and that the absorbed energy is rapidly converted to plasma thermal energy.

Appendix A

The solution to the MHD equations in the plasma regions is matched to the vacuum electric and magnetic fields through eqs. (22)-(23). In this appendix we perform this matching and derive an expression for the vacuum potential produced by the externally applied vacuum forces.

We express the perturbed vacuum magnetic field $\delta \underset{\sim}{B}_v$ as $\nabla\phi$, where ϕ is the magnetic potential which satisfies Laplace's equation in the vacuum region. After Fourier and Laplace transforming according to eq. (39), we write the solution for $\hat{\phi}$ in two parts as follows,

$$\hat{\phi} = c_1\, I_m(|k|r) + c_2\, K_m(|k|r) \quad , \quad r_p \le r \le r_c \quad , \tag{A1}$$

$$\hat{\phi} = d_1\, I_m(|k|r) + d_2\, K_m(|k|r) \quad , \quad r_c \le r \le r_w \quad , \tag{A2}$$

where I_m and K_m are the modified Bessel functions of first and second kind respectively, with argument $|k|r$ and m interpreted in the sense $|m|$. The constants c_1, c_2, d_1 and d_2 are determined by the boundary conditions at $r = r_p$, $r = r_c$, $r = r_w$, namely eqs. (22)-(26). Application of eqs. (24)-(26) yields the following set of equations for c_1, d_1, and d_2 in terms of c_2 and $\hat{J}_{s\theta}$:

$$d_1 + \alpha d_2 = 0 \tag{A3}$$

$$c_1\, I'_m(|k|r_c) - d_2[K'_m(|k|r_c) - \alpha\, I'_m(|k|r_c)] = - c_2\, K'_m(|k|r_c) \tag{A4}$$

$$d_2[K_m(|k|r_c) - \alpha\, I_m(|k|r_c)] - c_1\, I_m(|k|r_c) = c_2\, K_m(|k|r_c) + \frac{\mu_0\, \hat{J}_{s\theta}}{ik} \tag{A5}$$

where

$$\alpha = \frac{K_m'(|k|r_w)}{I_m'(|k|r_w)} \quad , \tag{A6}$$

and the prime, ( )', on the Bessel functions refers to derivatives with respect to the argument $|k|r$. Note that $\alpha \to 0$ as $r_w \to \infty$.

Let us define the quantity q as follows,

$$q = \left.\frac{\phi}{\frac{d\phi}{dr}}\right|_{r=r_p} \quad . \tag{A7}$$

Using eq. (A7), the constant c_2 can then be expressed in terms of c_1 and q, and, after solving eqs. (A4) and (A5) for c_1 and d_2 and rearranging, the final expression for $\hat{\phi}$ can be written as

$$\hat{\phi} = \frac{f}{1-\alpha\chi_1} \left[I_m(|k|r) - \chi_1 K_m(|k|r)\right] \quad , \; r_p \leq r \leq r_c \quad , \tag{A8}$$

where,

$$\chi_1 \equiv \frac{I_m(|k|r_p) - |k|q \; I_m'(|k|r_p)}{K_m(|k|r_p) - |k|q \; K_m'(|k|r_p)} \quad , \tag{A9}$$

and,

$$f = - \operatorname{sgn}(k) \; i \; \mu_0 \; \hat{J}_{s\theta} \; r_c \; K_m'(|k|r_c) \left(1 - \alpha \frac{I_m'(|k|r_c)}{K_m'(|k|r_c)}\right) \tag{A10}$$

Equations (A8) and (A10) yield eqs. (62) to (64).

Figure Captions

Fig. 1. Schematic of the plasma-vacuum-coil-wall configuration.

Fig. 2. Friedrichs' diagram for MHD waves in an infinite uniform plasma.

Fig. 3. Wave front diagram for the three MHD waves whose phase velocities are shown in Fig. 2.

Fig. 4. Dispersion diagram for the three MHD waves of Figs. 2 and 3 illustrating resonance and cut-off features in an infinite uniform plasma.

Fig. 5. Schematic of the function $r_0(\omega)$ shown as a function of frequency ω for both the Alfvén and cusp branches.

Fig. 6. Typical branch cuts and branch points of the function $\psi_s(r,\omega)$ in the complex ω plane (b) for the resonant frequency profile $\omega_j^2(r')$ ($j \equiv A$ for Alfvén mode and $j \equiv C$ for cusp mode) shown in (a).

Fig. 7. Deformed Laplace contour used for inverting the Laplace transform of $r\hat{\xi}(r,\omega)$. Exposed roots ω_s^{α}, ω_s^{β} in the complex plane correspond to damped surface waves while those on the ω_r axis ω_m^{α}, ω_m^{β}, ω_m^{γ} correspond to stable magneto-acoustic waves.

Fig. 8. Radial dependence of pressure, P, magnetic fields, B_θ/μ, B_z and density ρ in normalized form for the ST Tokamak plasma.

Fig. 9. Radial dependence of Alfvén and cusp, ω_A and ω_C respectively, frequency continuum for the plasma profiles of Fig. 8. The cusp frequencies are multiplied by a factor of 10. In the figure, m = 1.

Fig. 10. Radial dependence of pressure, magnetic field and density in normalized form for a Scyllac plasma, $\beta = 0.5$ on axis.

Fig. 11. Radial dependence of Alfvén and cusp continuum frequencies, $\tilde{\omega}_A$ and $\tilde{\omega}_C$, for Scyllac plasma. The β on axis equals 0.5 and m = 1 has been assumed.

Fig. 12 Radial dependence of Alfven and cusp continuum frequencies, $\tilde{\omega}_A$ and $\tilde{\omega}_C$, for reversed bias θ-pinch. $\beta = 0.5$ and m = 1 has been assumed.

Fig. 13 Real part of coil impedance, Z_R, versus frequency, f, for ST plasma. Results for m = 1 and 2 coils shown for wave length equal to 60 cm.

Fig. 14 Real part of coil impedance, Z_R, as a function of frequency, f, for Ormak A discharge. $\tilde{k} = .287$ and m = 1, 2 and 3.

Fig. 15 Real part of coil impedance, Z_R, as a function of frequency, f, for Ormak B discharge. $\tilde{k} = .287$ and m = 1, 2, and 3.

Fig. 16 Real part of coil impedance, Z_R, as a function of frequency, f, for Ormak B discharge. $\tilde{k} = .594$ and m=1,2,3.

Fig. 17a Real part of coil impedance, Z_R, as a function of frequency, f, for Ormak A profiles and variable wall position. m = 1, $\tilde{k} = .287$ and r_w/r_c varied from 10 to 1.1. The value of $r_c/r_p = 1.0$.

Fig. 17b Imaginary part of coil impedance, Z_I, as a function of frequency, f, for Ormak A profiles and variable wall position.

Fig. 18a Real part of coil impedance, Z_R , as a function of frequency, f, for Ormak A profiles and variable wall position. m = 1, k = .287 and r_w/r_c varied from 10 to 1.1. The value of $r_c/r_p = 1.5$.

Fig. 18b Imaginary part of coil impedance, Z_I , as a function of frequency, f, for Ormak A profiles and variable wall position.

Fig. 19 Real part of impedance, Z_R , versus frequency, f, for Scyllac profiles. m = 1, wave length = 33 cm, $\beta = 0.5$ and $r_c/r_p \approx 1.5$.

References

Chen, L., and Hasegawa, A. (1974) Phys. Fluids 17, 1399.

Cumberbatch, E. (1962) J. Aerospace Sci. 29, 1476.

England, A., personal communication.

Furth, H.P. (1959) University of California Rad. Lab. Engineering Note UCRL-5423-T.

Goedbloed, H., and Sakanaka, P. (1974) Phys. Fluids 17, 9191.

Golovato, S.N., Shohet, J.L., and Tataronis, J.A. (1976) Phys. Rev. Letts. 37, 1272.

Gould, R., Proceedings of U.S.-Australia Workshop on Plasma Waves, Report SR-6, Texas Tech. (1975).

Grad, H. (1969) Phys. Today 22, 34.

Grad, H. (1973) Proc. Nat. Acad. Sci. 70, 3277.

Grossmann, W., Kaufmann, M., and Neuhauser, J. (1973) Nuclear Fusion 13, 462.

Grossmann, W., and Tataronis, J.A. (1973) Z. Physik 261, 203 and 217.

Hasegawa, A., and Chen, L. (1975) Phys. Rev. Letts. 35, 370.

Hosea, J., personal communication.

Kappraff, J., Tataronis, J.A., and Grossmann, W. (1975) in Proc. of the Seventh European Conference on Controlled Fusion and Plasma Physics (Lausanne, Switzerland, 1975) Paper 158.

Kappraff, J., and Tataronis, J.A. (1977) to be published in J. Plasma Phys.

Pochelon, A., and Keller, R. (1977) Bericht der Herbsttagung der Schweizerischen Physikalischen Geselleschaft 50, 172.

Shohet, J.L., Golovato, S.N., and Tataronis, J.A. (1976) Proc. of the 1975 Sherwood Theory Meeting, Madison, Wisc., also (1977) IEEE Trans. on Plasma Sci., Vol. PS-5, No. 2.

Tataronis, J.A., and Grossmann, W. (1971) 1971 Annual Report of the Max-Planck-Institut für Plasmaphysik (Garching, W. Germany, 1971), pages 26-27 and page 164.

Tataronis, J.A., and Grossmann, W. (1972) in Proc. of the Second Conference on Pulsed High Beta Plasmas, (Garching, W. Germany, 1972) B5 and B6.

Tataronis, J.A., and Grossmann, W. (1974) in Proc. of the Second Topical Conference on RF Plasma Heating (Lubbock, Texas, 1974) paper A-6.

Tataronis, J.A. (1975) J. Plasma Phys. 13, 87.

Tataronis, J.A., and Grossmann, W. (1976) Nucl. Fusion 16, 667.

Thompson, W.B., private communication.

Ubroi, C. (1972) Phys. Fluids 15, 1673.

Uo, K., et al (1976) in Proc. of Plasma Physics and Controlled Nuclear Fusion Research, IAEA-CN-35/D4 (Tokyo, 1976).

Figure 1

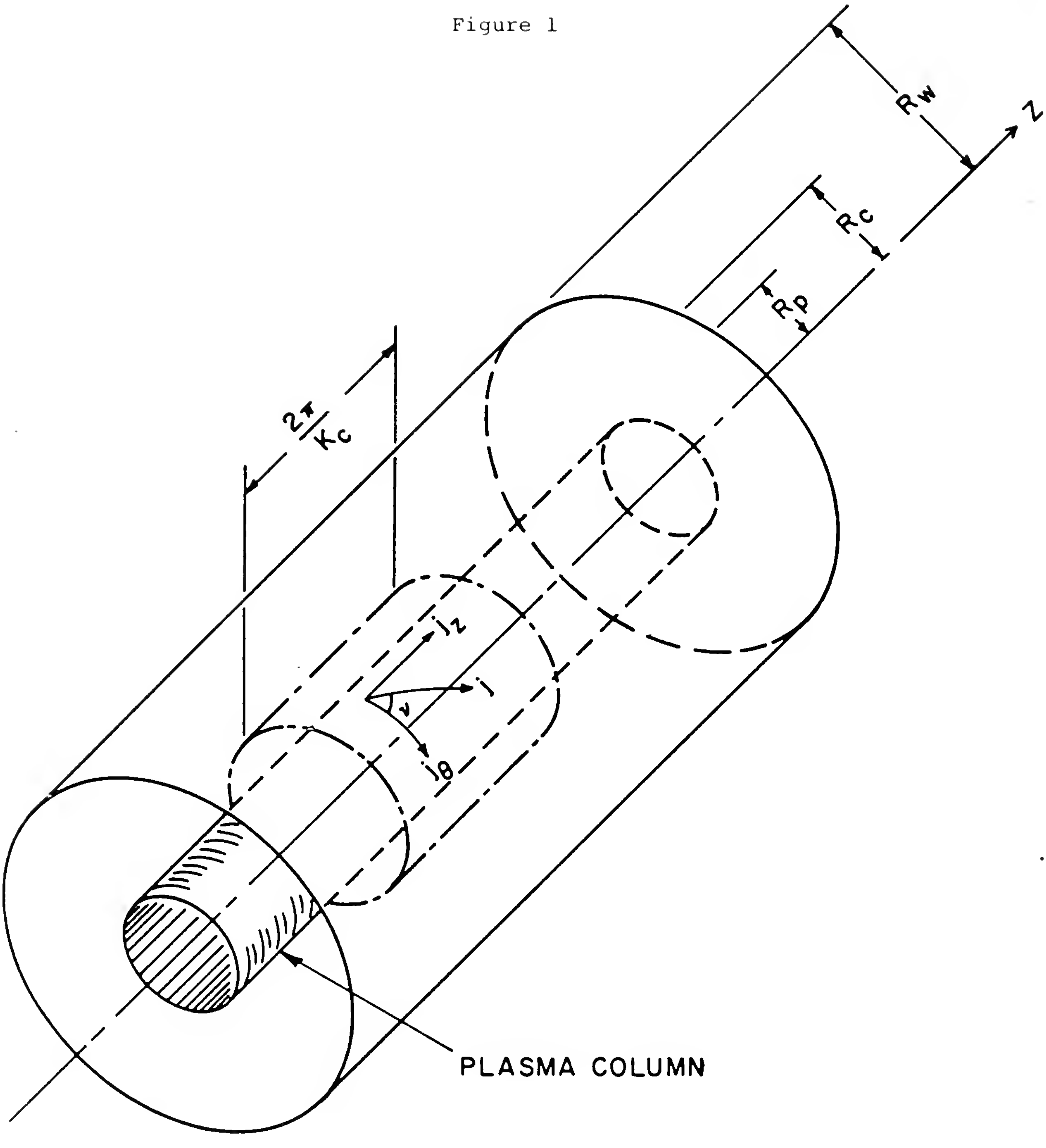

Figure 2

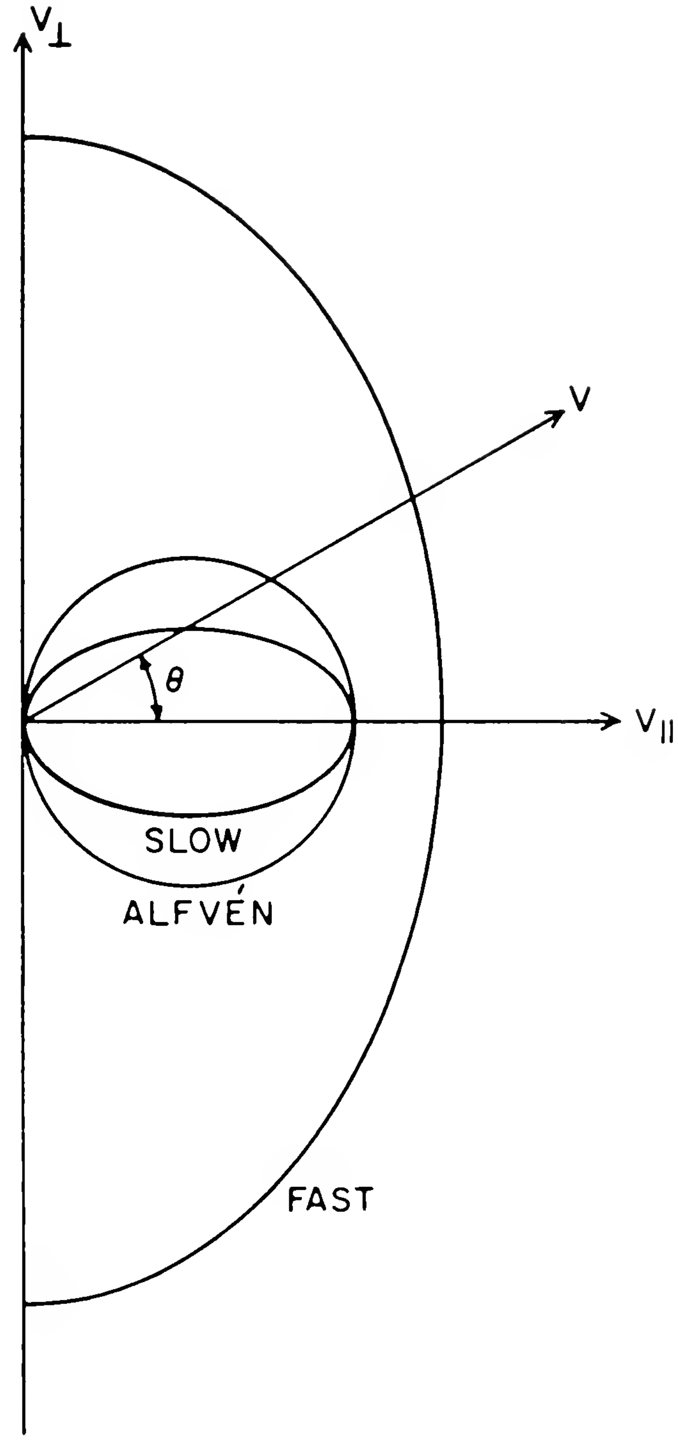

Figure 3

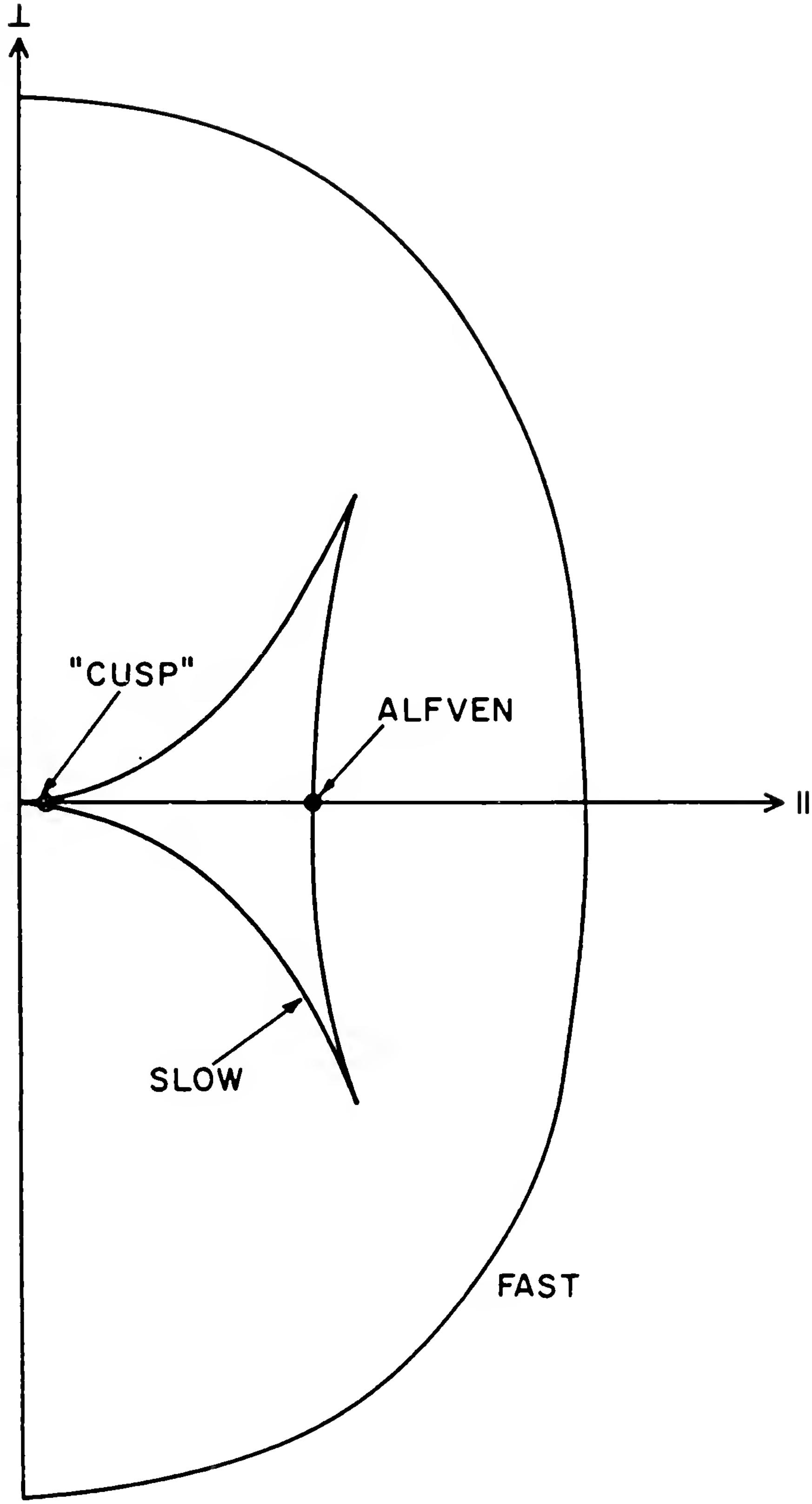

Figure 4

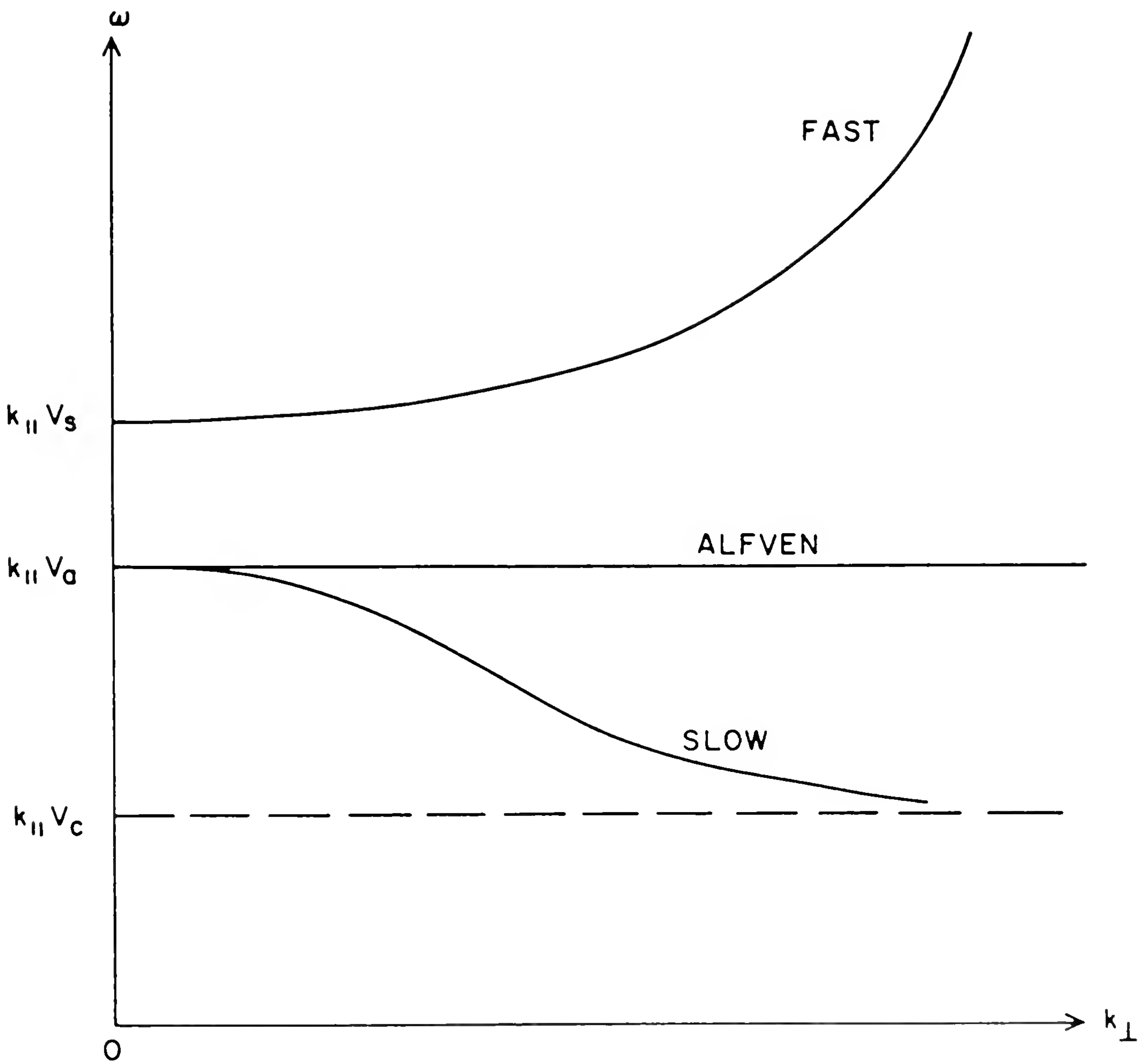

ω
FAST
$k_{\parallel} V_s$
ALFVEN
$k_{\parallel} V_a$
SLOW
$k_{\parallel} V_c$
0
$k_{\perp}$

Figure 5

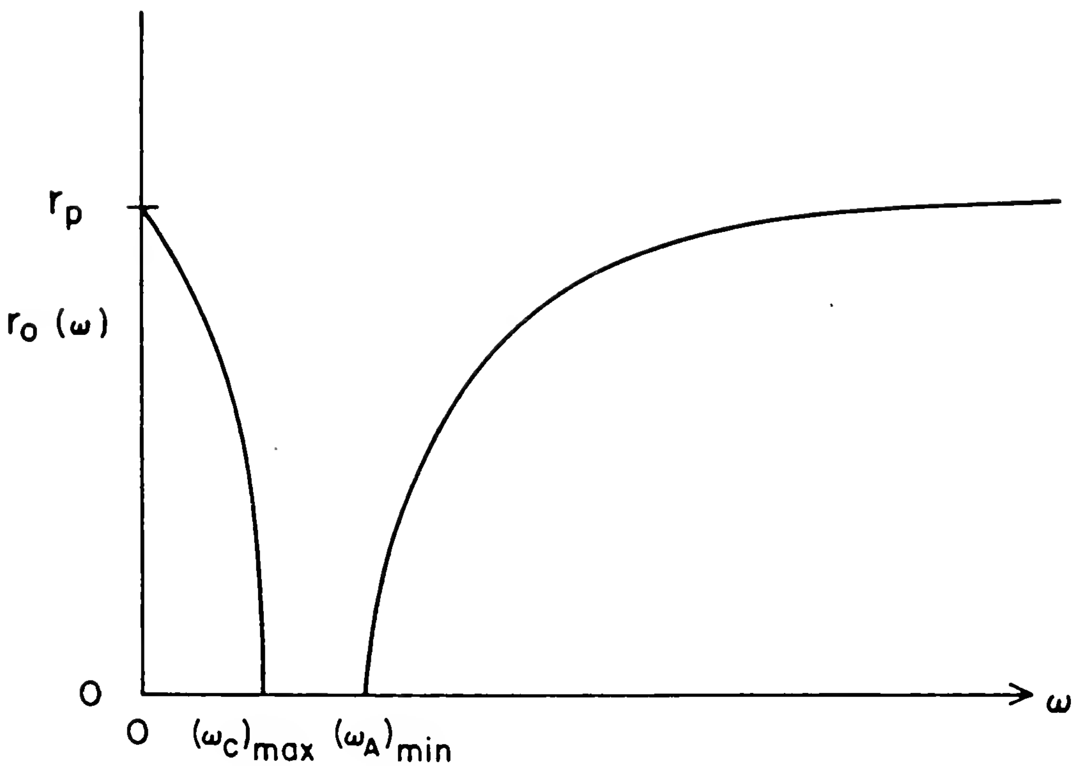

Figure 6

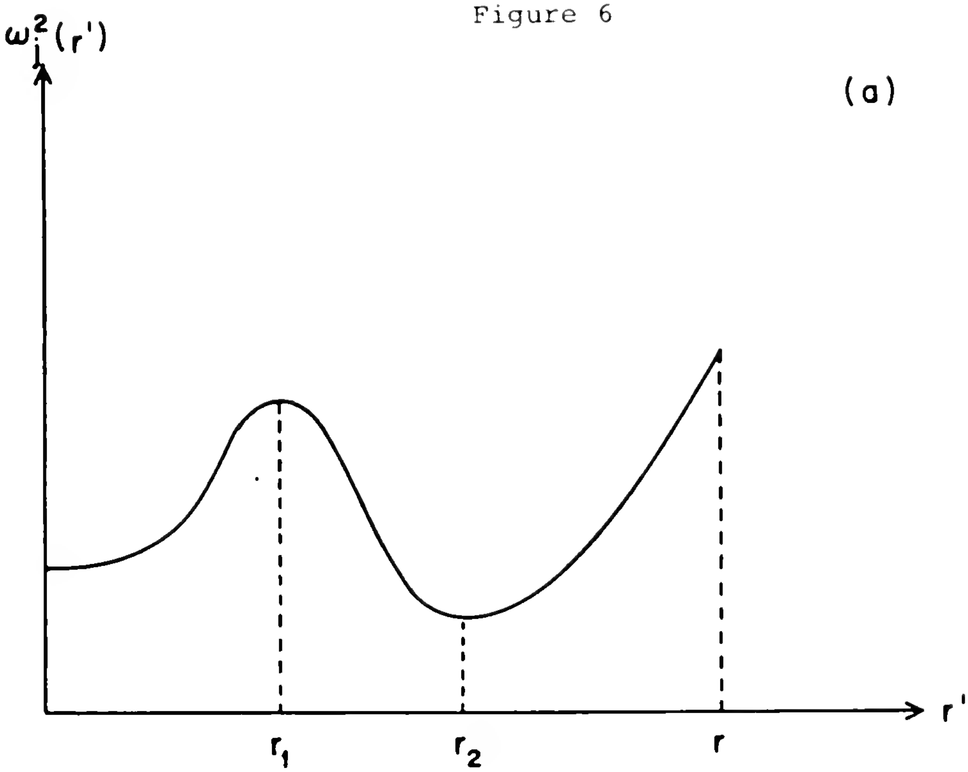

$\omega_j^2(r')$
(a)
r'
r_1
r_2
r

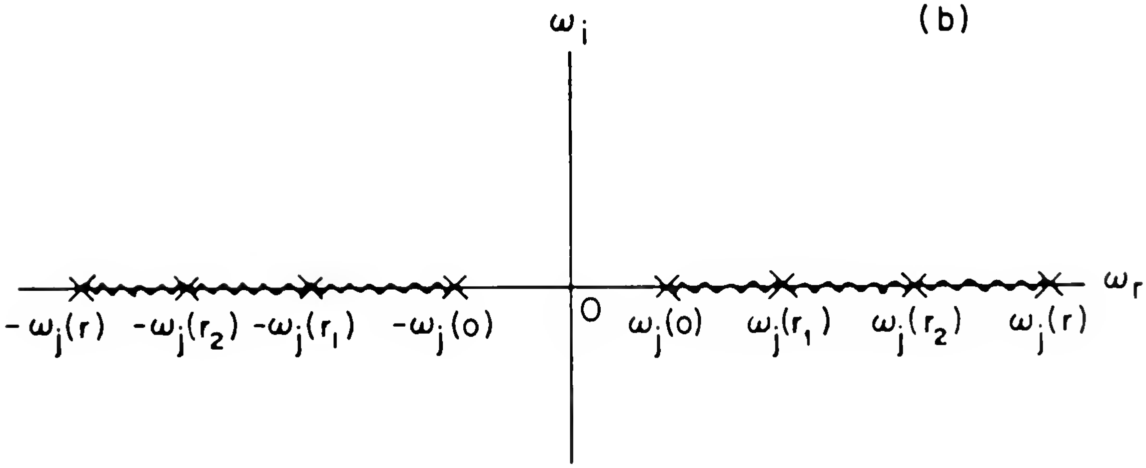

ω_i
(b)
ω_r
$-\omega_j(r)$
$-\omega_j(r_2)$
$-\omega_j(r_1)$
$-\omega_j(0)$
0
$\omega_j(0)$
$\omega_j(r_1)$
$\omega_j(r_2)$
$\omega_j(r)$

Figure 7

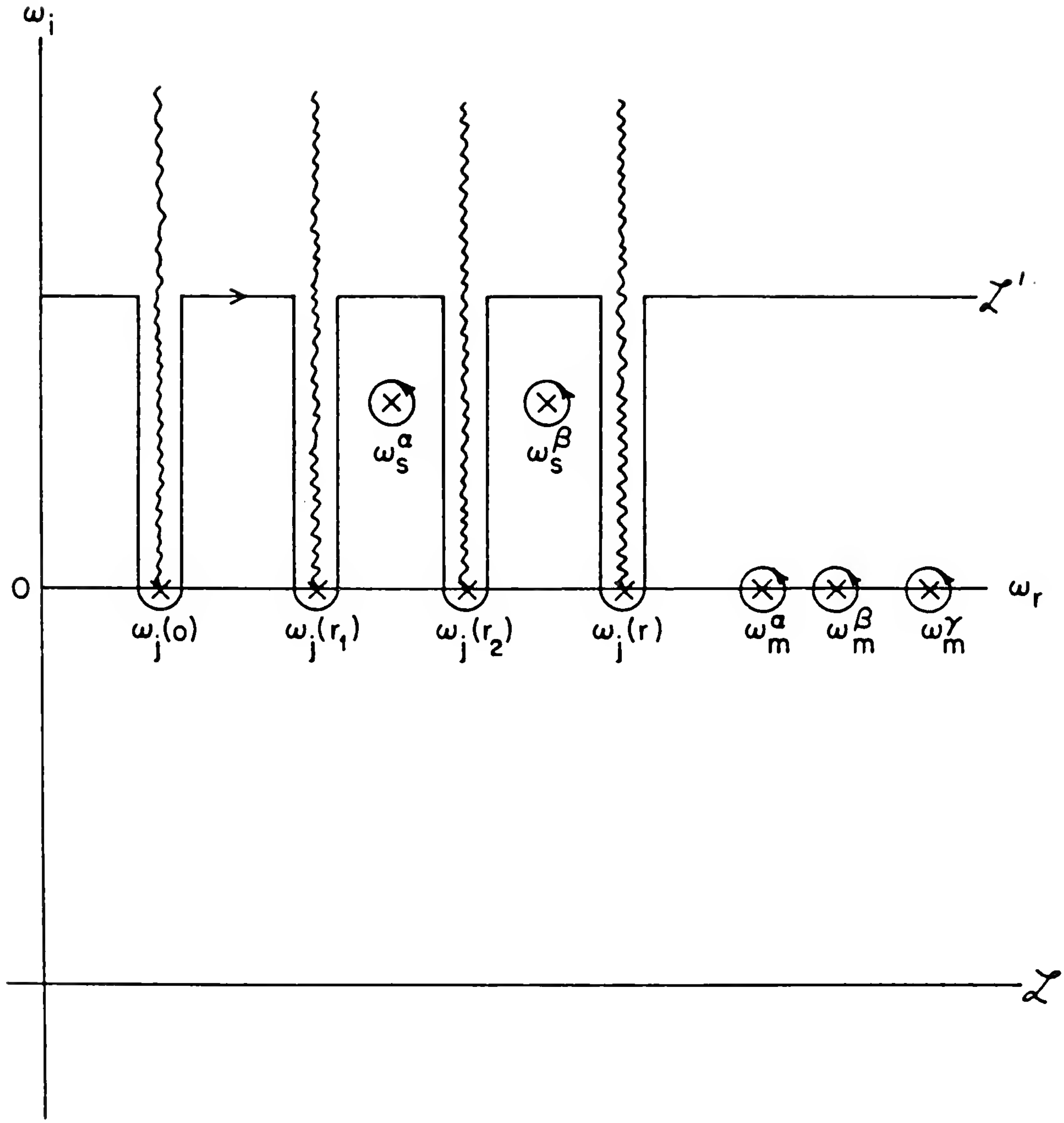
ω_i
$\mathcal{L}'$
ω_s^α
ω_s^β
0
ω_r
$\omega_j(o)$
$\omega_j(r_1)$
$\omega_j(r_2)$
$\omega_j(r)$
ω_m^α
ω_m^β
ω_m^γ
$\mathcal{L}$

Figure 8

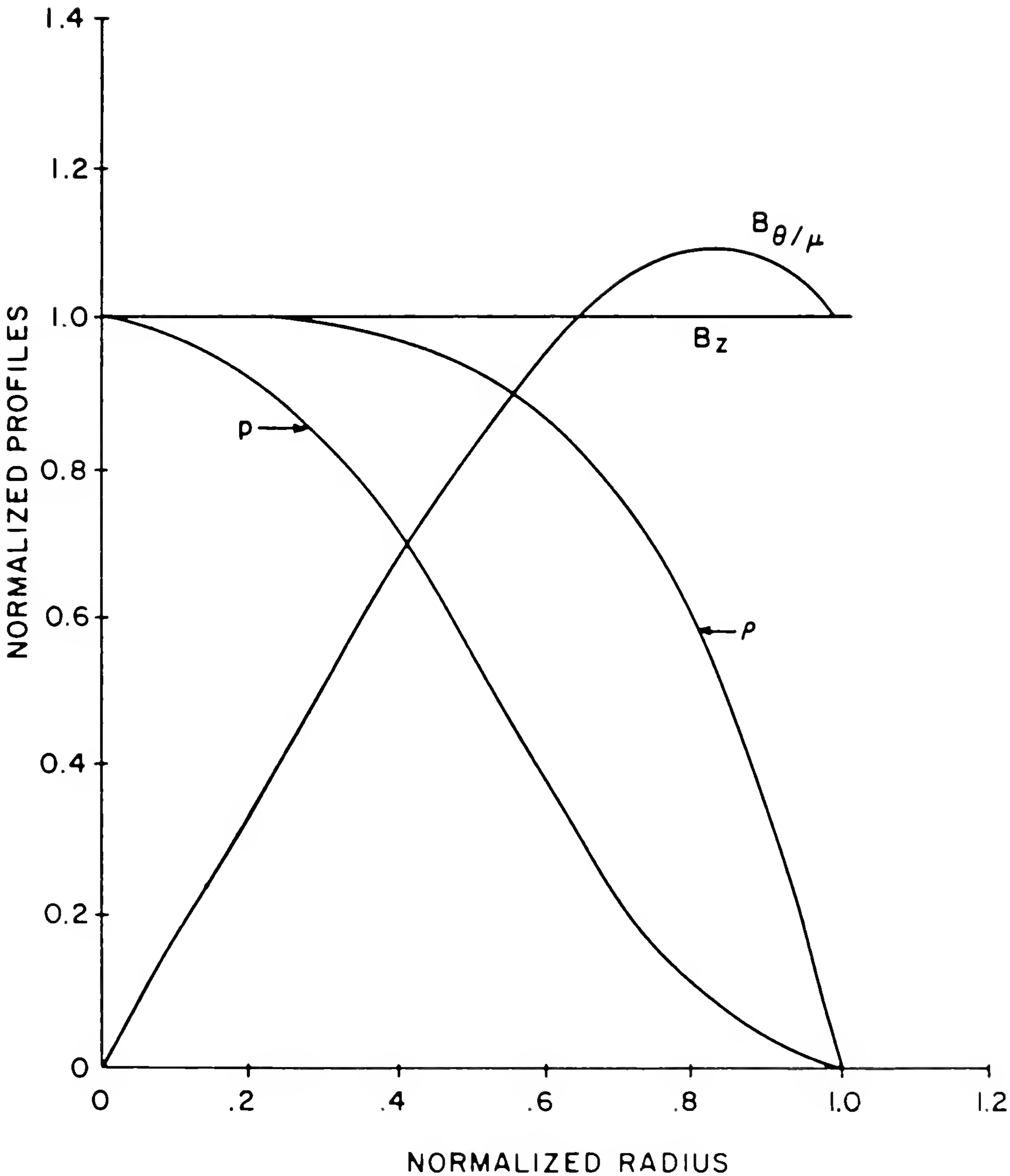

1.4
1.2
1.0
0.8
0.6
0.4
0.2
0
NORMALIZED PROFILES
$B_{\theta/\mu}$
B_z
p
ρ
0
.2
.4
.6
.8
1.0
1.2
NORMALIZED RADIUS

Figure 9

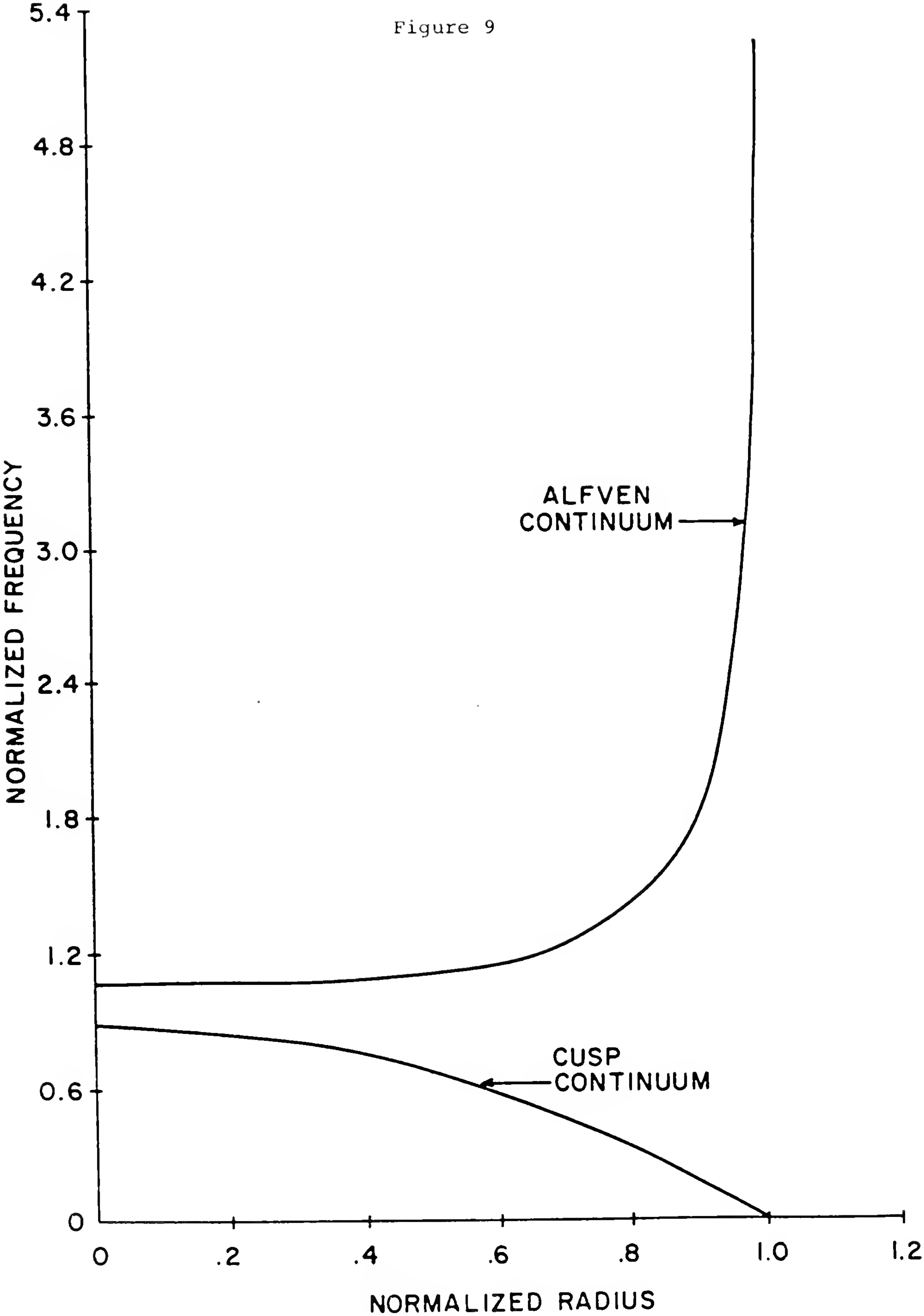
5.4
4.8
4.2
3.6
3.0
2.4
1.8
1.2
0.6
0
NORMALIZED FREQUENCY
ALFVEN
CONTINUUM
CUSP
CONTINUUM
0
.2
.4
.6
.8
1.0
1.2
NORMALIZED RADIUS

Figure 10

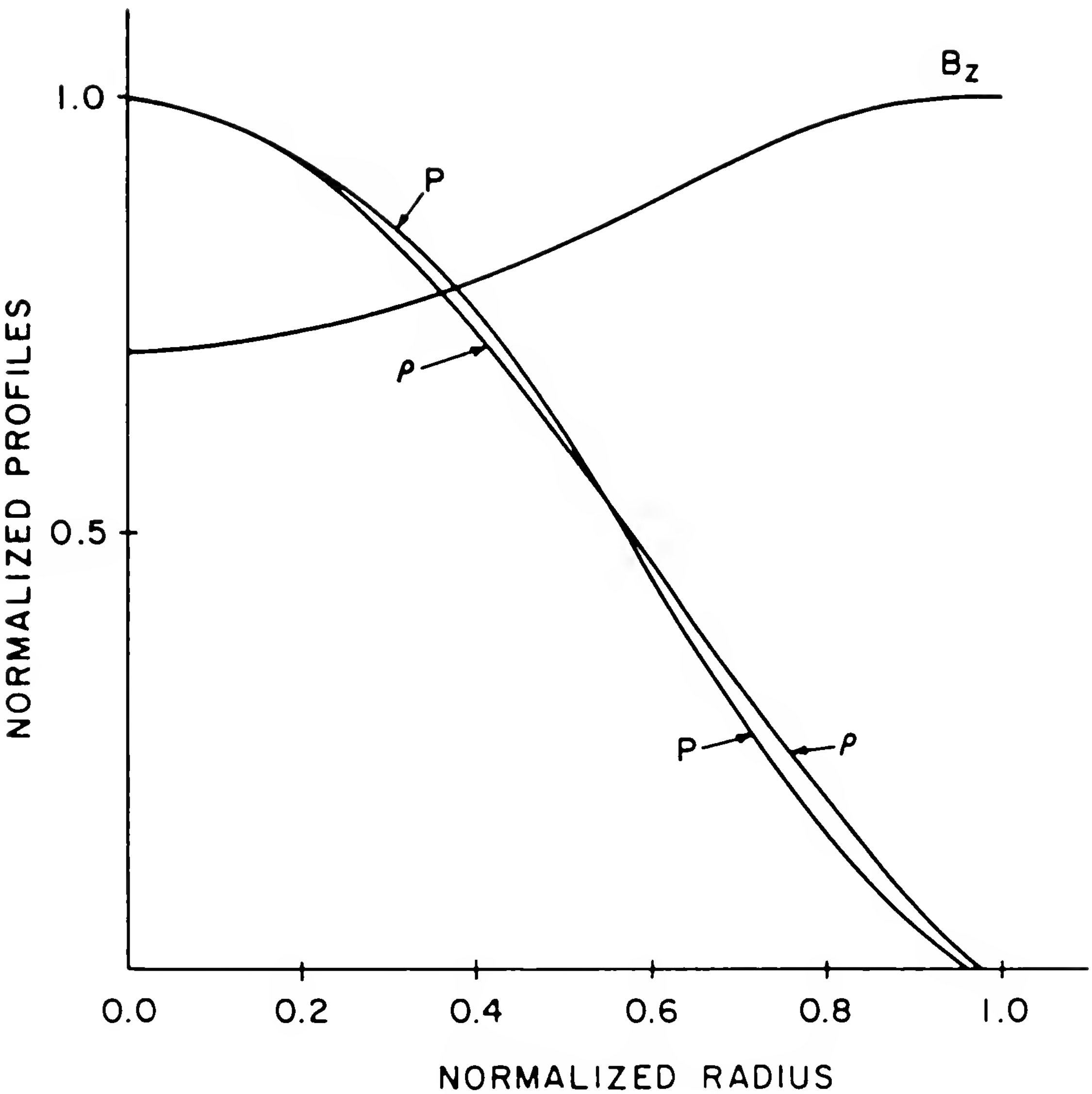

B_z
1.0
0.5
P
ρ
P
ρ
0.0
0.2
0.4
0.6
0.8
1.0
NORMALIZED PROFILES
NORMALIZED RADIUS

Figure 11

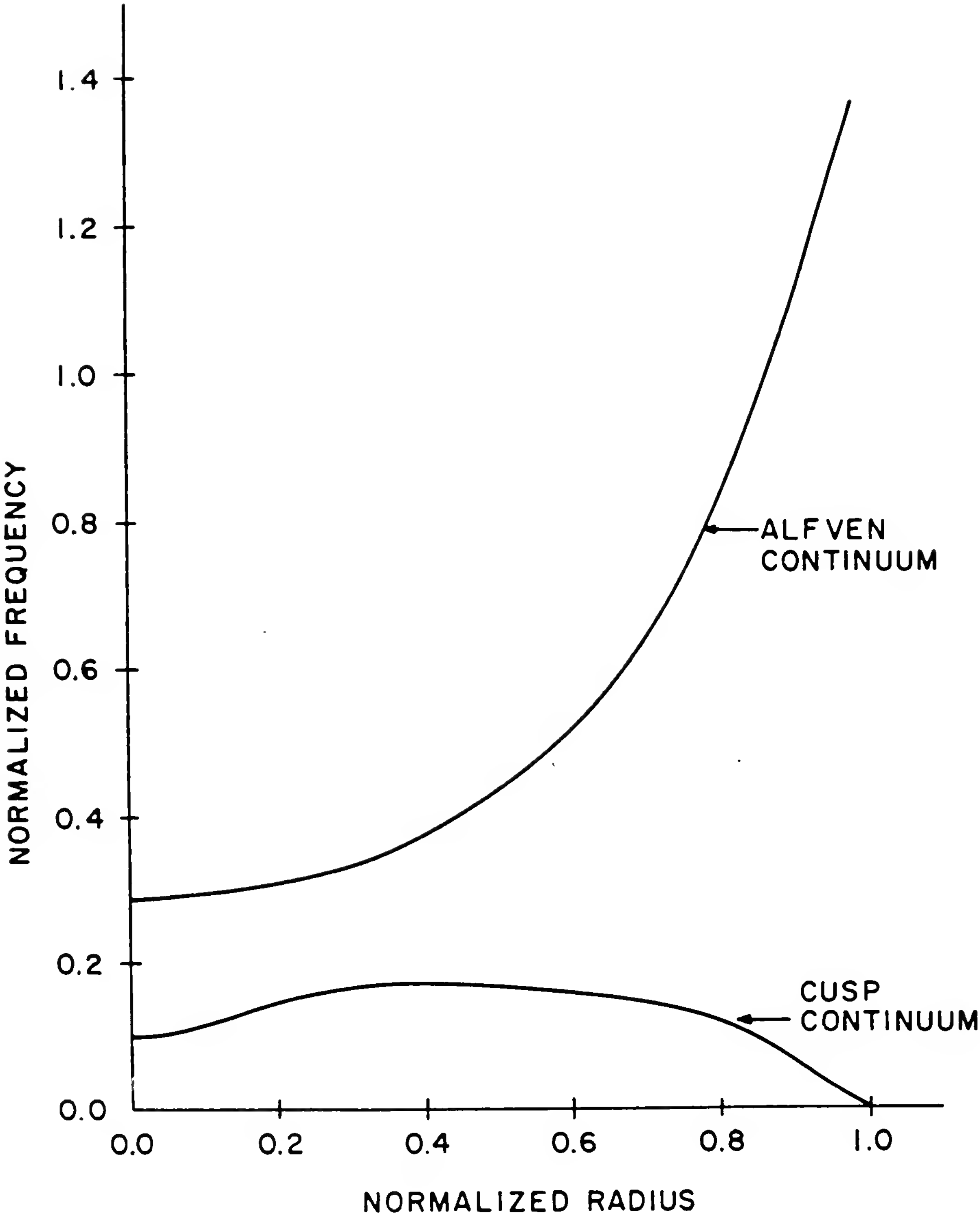
1.4
1.2
1.0
0.8
0.6
0.4
0.2
0.0
NORMALIZED FREQUENCY
ALFVEN
CONTINUUM
CUSP
CONTINUUM
0.0
0.2
0.4
0.6
0.8
1.0
NORMALIZED RADIUS

Figure 12

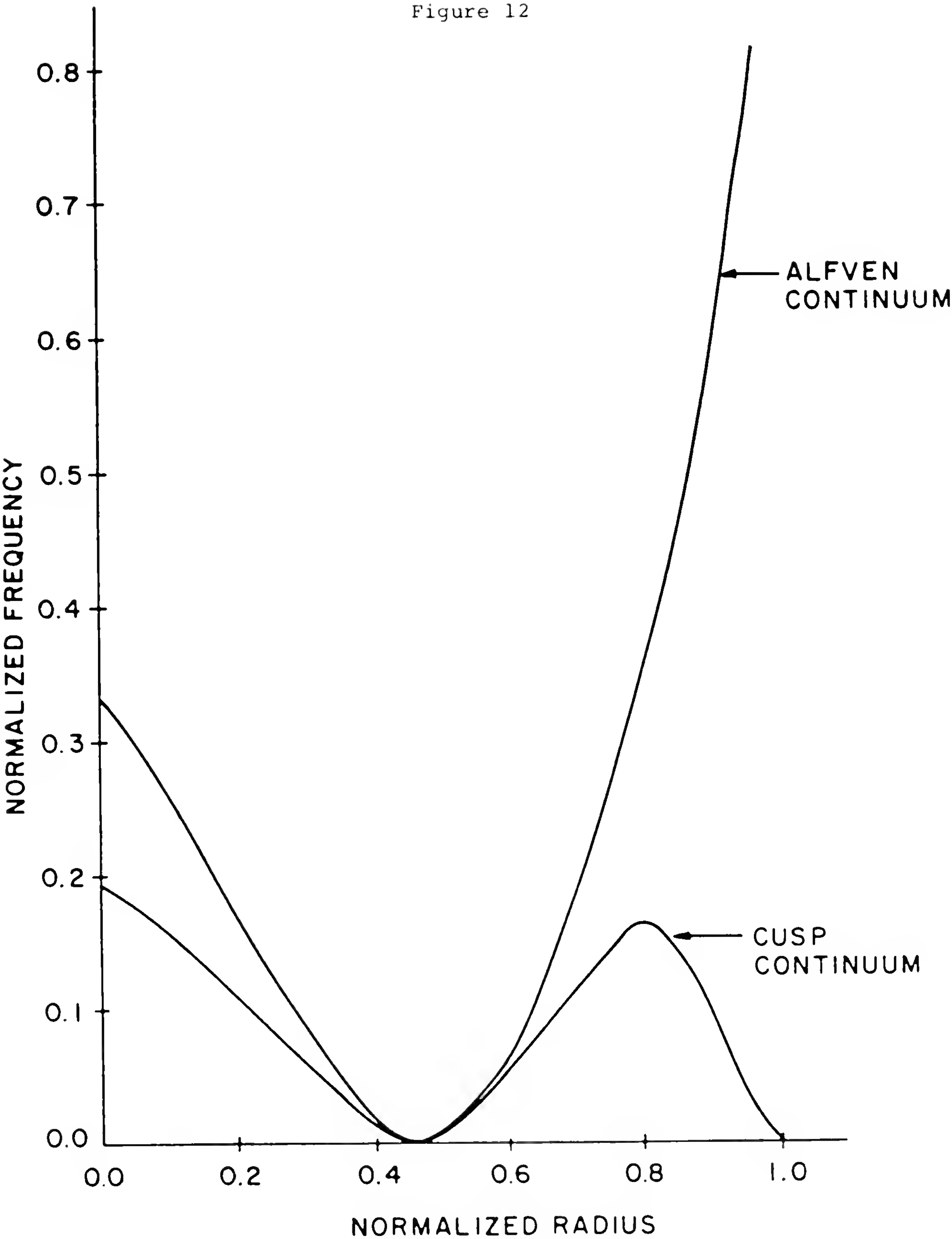

0.8
0.7
0.6
0.5
0.4
0.3
0.2
0.1
0.0
NORMALIZED FREQUENCY
ALFVEN CONTINUUM
CUSP CONTINUUM
0.0
0.2
0.4
0.6
0.8
1.0
NORMALIZED RADIUS

Figure 13

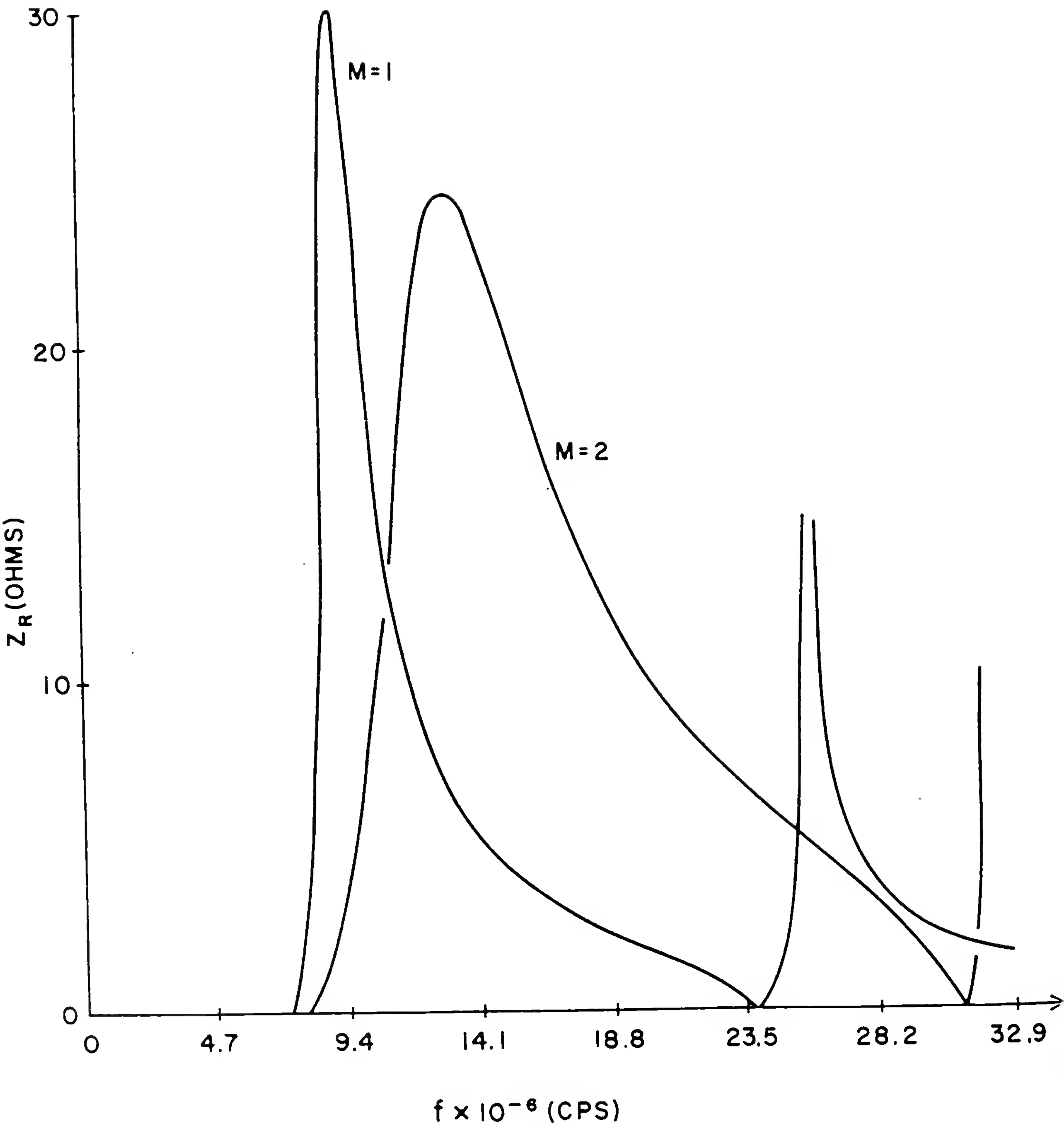

Figure 14

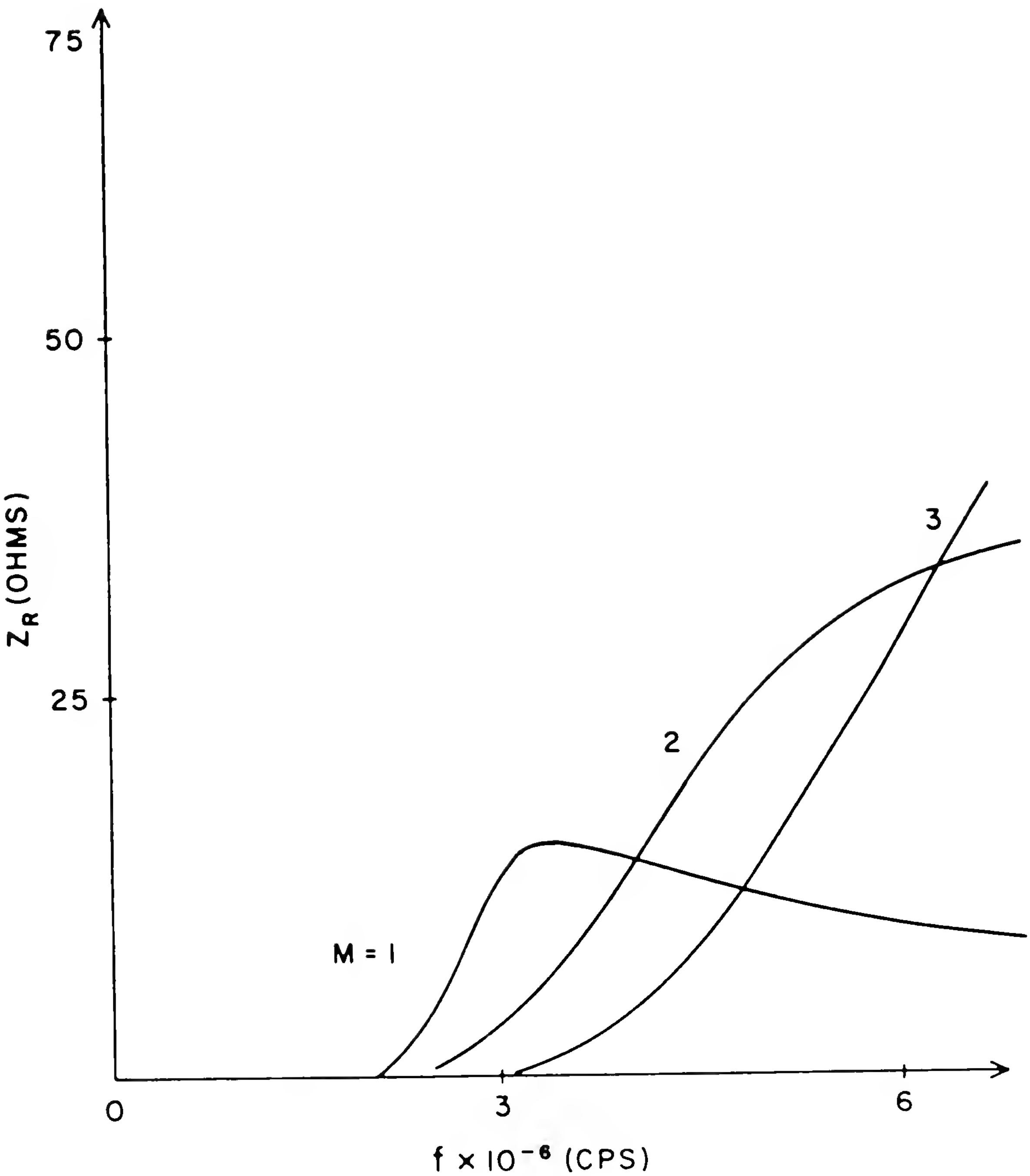

Figure 15

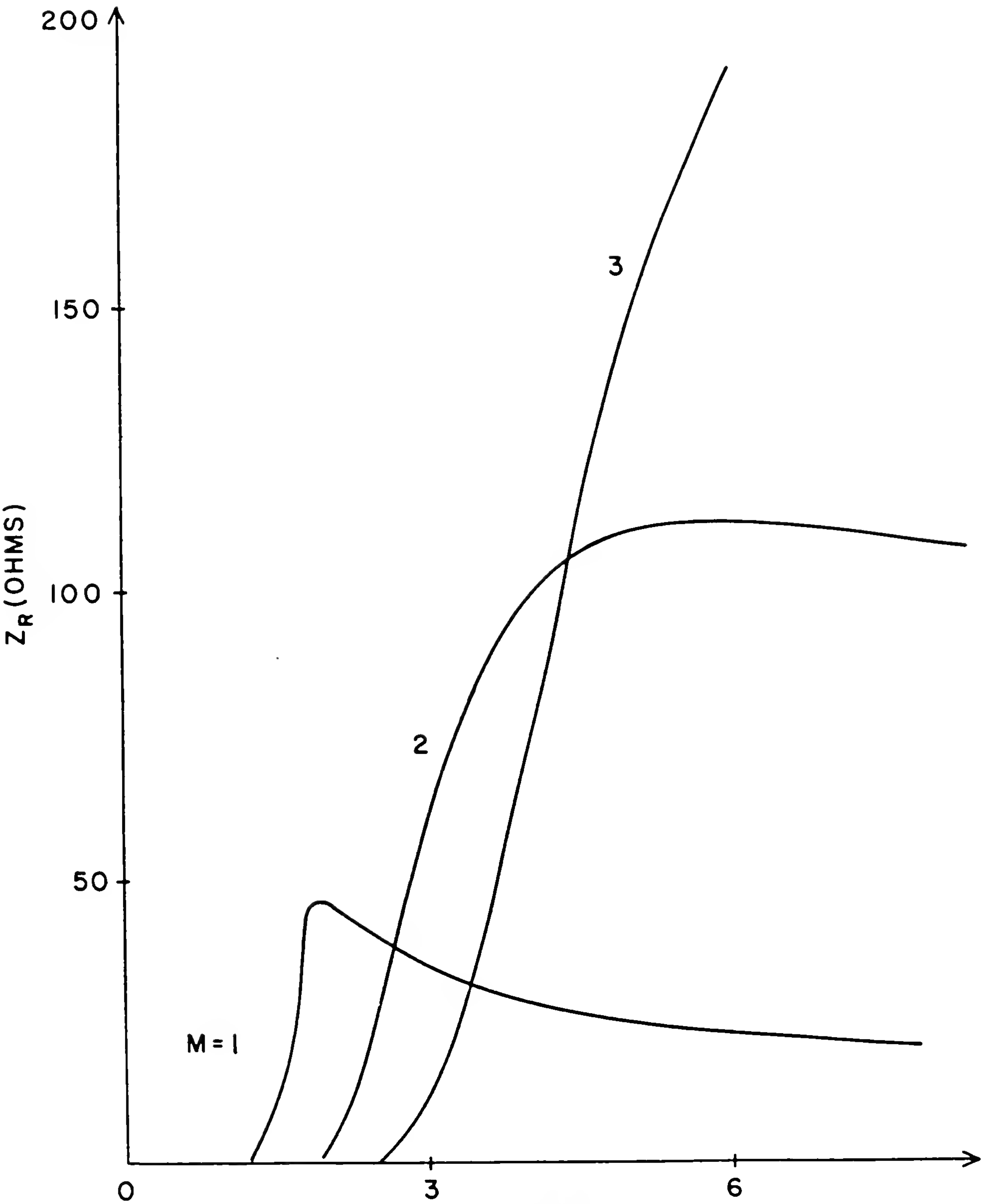

Figure 16

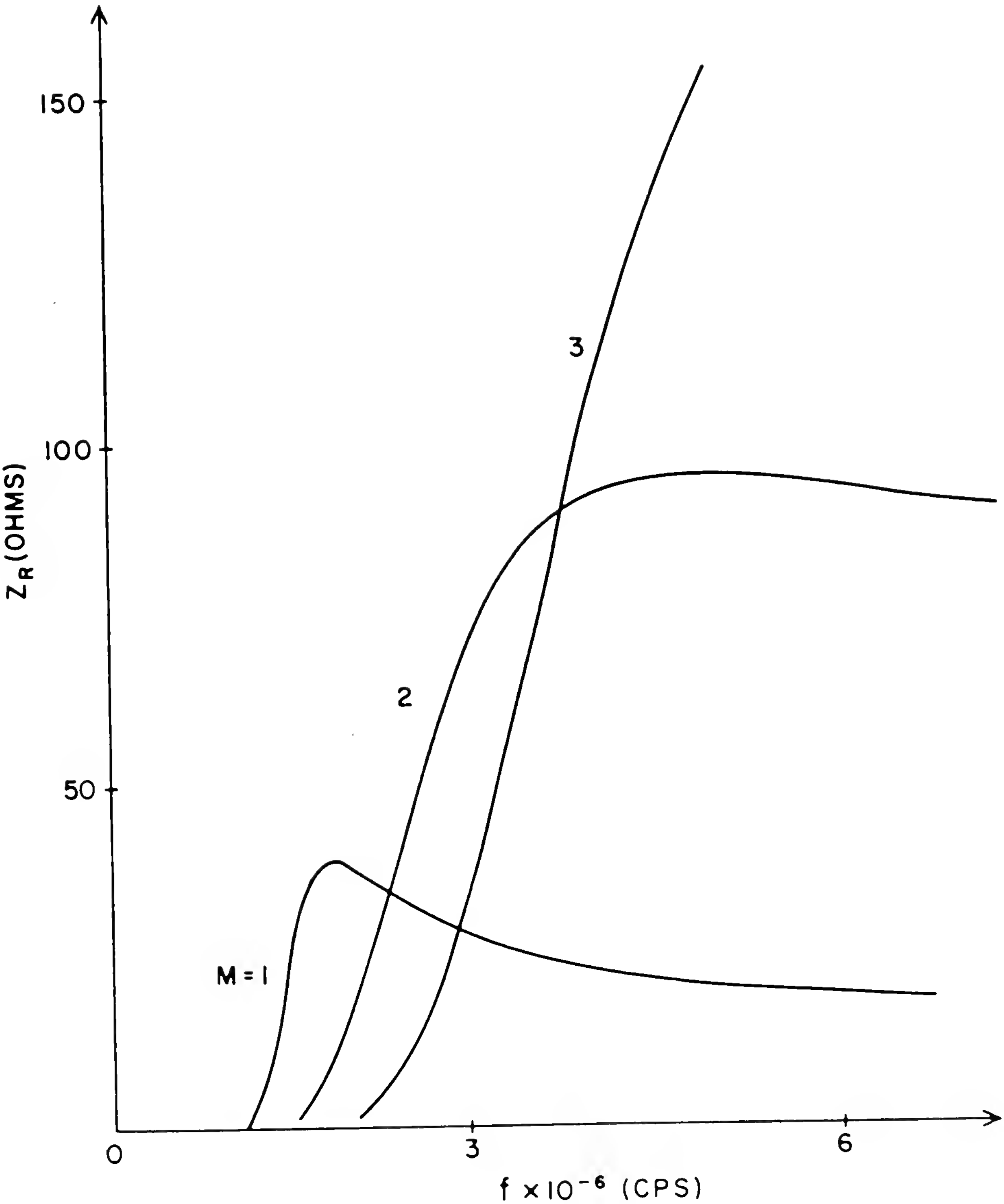

Figure 17a

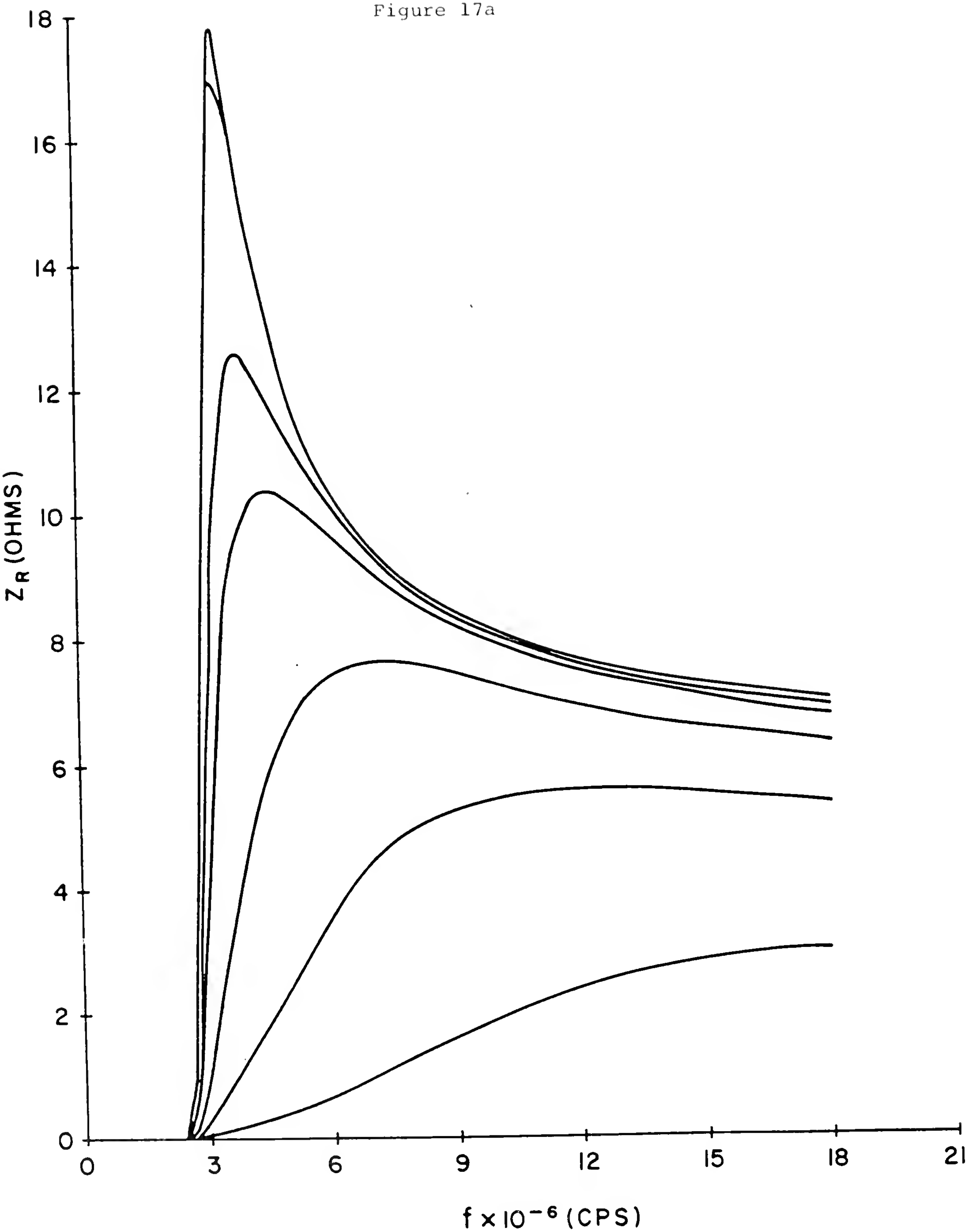

Figure 17b

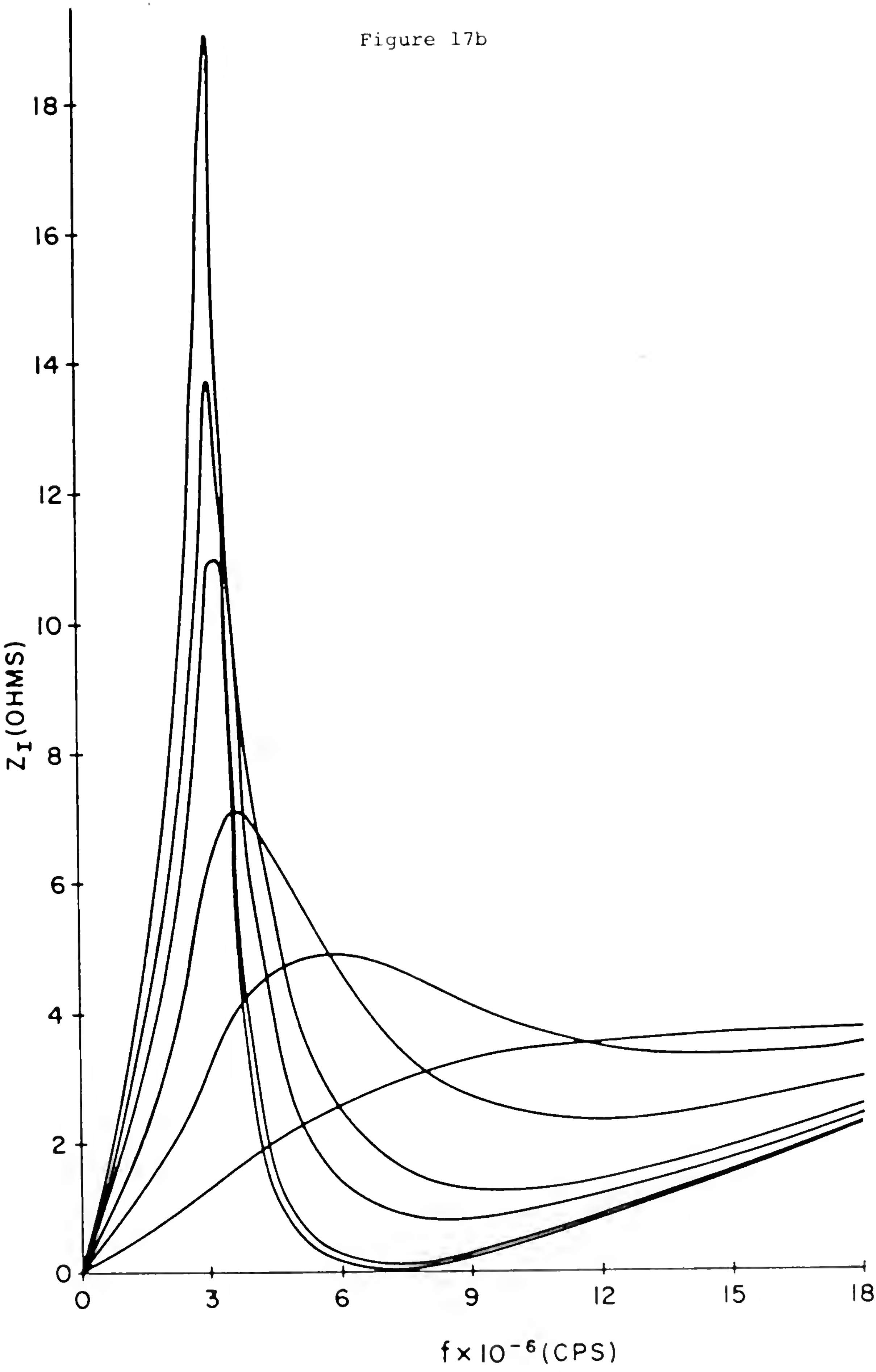

Figure 18a

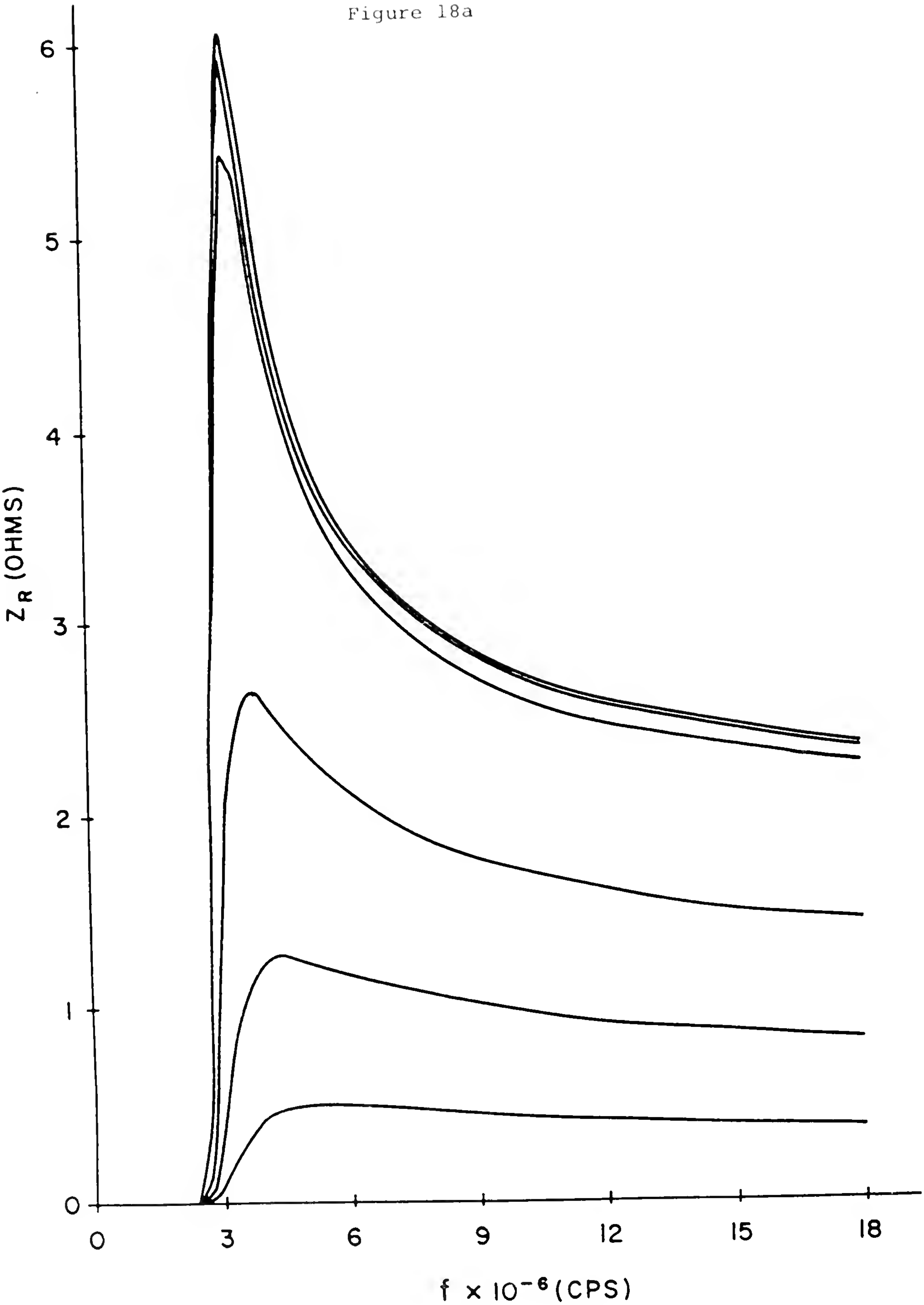

Figure 18b

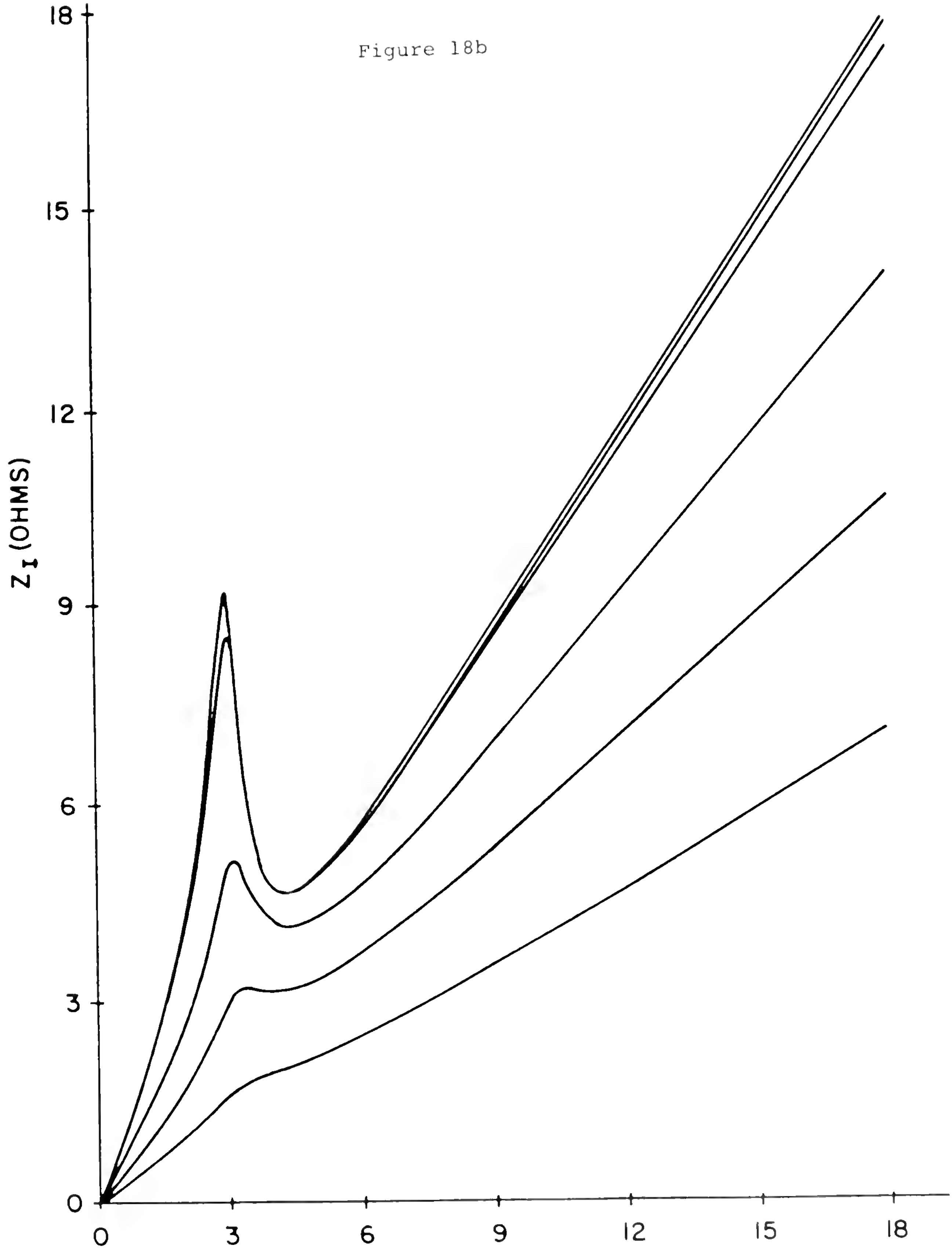

Figure 19